MEMOIRS

OF THE

COLLEGE OF SCIENCE

UNIVERSITY OF KYOTO

SERIES A

VOL. XXVII, No. 4

July 1956

KYOTO

Digitized by the Internet Archive
in 2024

https://archive.org/details/memoirs-faculty-science-kyoto-phys-astro-geophys-chem_1956-07_27_4

MEMOIRS OF THE COLLEGE OF SCIENCE, University of Kyoto, Series A,
Vol. XXVII, No. 4, Article 1, 1956

CHANGES OF ABSORPTION BANDS OF ALKALI-HALIDE CRYSTALS COLOURED IN SEVERAL CONDITIONS

BY

Hisao YAGI

(Received March 1, 1956)

ABSTRACT

When the alkali-halide crystals were coloured in various conditions, two more new bands were found. The one exists between F-band and K-band, and its nature may be colloids. The other exists between U-band and K′-band, and its nature is quite similar to K-band.

1. Introduction

V-bands of coloured alkali-halide crystals consist of $V_1 \cdots V_7$-absorption bands as reported by H. Dorendorf (**1**), and on the other hand, in the same region, K- and K′-bands were found in our laboratory (**2**), but K-band appears remarkably in the crystals coloured by electrolysis. When we coloured the crystals in various conditions, two more new bands were found. The one is on the side of longer wavelength than K-band, and the other on the side of shorter wavelength than K′-band. They are called W-band and K_2-band respectively. Only the existence of K_2- and W-bands was reported by M. Hacskaylo (**3**). The nature of K_2-band is similar to that of K-band, while the nature of W-band is different from that of known bands.

2. Experimental procedures

The NaCl, KCl and KBr crystals used in these experiments were grown in our laboratory (**4**) by Kyropoulos' method. In order to subject crystals to electrolysis, they were mounted in a furnace in a manner as shown in Fig. 1. (This is called "pointed-electrode method".) A crystal was supported between two iron rods which served as a part of electrical circuit supplying the current for electrolysis. The one rod (A) is pointed sharply at its end and acts as cathode. The other (B) contacts the crystal with the carbon plate covered with platinum foil and acts as anode. All parts except the furnace can be evacuated. Current is supplied by a 450 volts power supply with a 500 KΩ resistor.

After inserting a crystal in the furnace, the temperature of the furnace was first raised up to 450°～500°C, and the current was supplied, and coloured cloud was made electrolytically in the crystal. (This coloured condition is called "F-coloured".)

Then, the temperature of the furnace was brought down to 350°~400°C, and the coloured cloud in the crystal was removed by reversing the polarity of the current. (This coloured condition is called "K-coloured".)

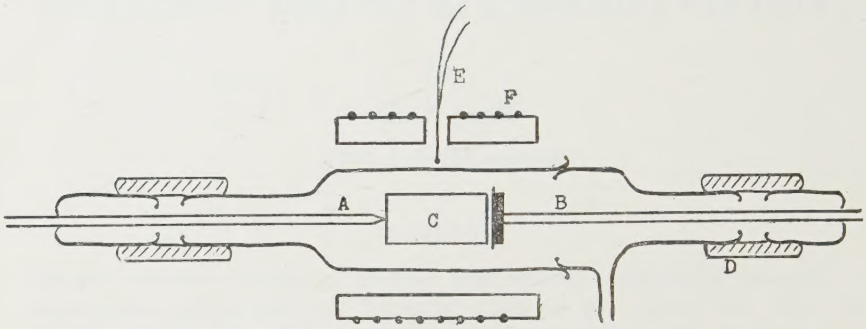

Fig. 1. Arrangement for subjecting crystals to electrolysis.
A: cathode, B: anode, C: crystal, D: rubber,
E: thermocouple, F: furnace.

For the irradiation with X-rays, a Mazda Sealex tube was used which was operated at a voltage of 30 KV D.C. and a current of 8 mA. During the irradiation, the temperature of the crystal was variable from 20°C to 300°C.

As a general rule, the crystals used were freshly cleaved on all sides at the last possible moment before starting an experiment.

The absorption spectra of the crystals were obtained with a Beckman Quartz Spectrophotometer Model DU which permitted measurements in the spectral range of 210~1000 mμ.

3. Results obtained

Generally speaking, in the case of X-ray coloured crystals, V_2-band appears remarkably and then appear K-, K'- and V_3-bands at room temperature. In the case of electrolytically coloured crystals, however, V-band does not appear (**5**)*, but U-, K-, K_2-, K'- and W-bands appear in respective conditions. The spectral location of the absorption bands in the region between F-band and U-band is shown in Table 1.

Table 1. The spectral location of the absorption bands.
(unit: mμ)

Bands / Crystals	U	V_3	V_2	K_2	K'	K	W	F
NaCl	192	210	222	230	258	293	328	465
KCl	215	215	232	345	267	307	348	560
KBr	230	232	265	280	290	320	375	631

* Recently V-band was also found by Y. Uchida and Y. Nakai by a special method.

A. *W-band*

When the crystals are electrolyzed in vacuum, W-band appears on the side of longer wavelength than K-band. W-band of NaCl crystal F-coloured at relatively lower temperature and then K-coloured at relatively higher temperature is shown in Fig. 3. When irradiated by the light lying in this band, this band did not change, but when irradiated by the light lying in K-band, only K-band was reduced. That is, W-band is not destroyed by the light lying in itself.

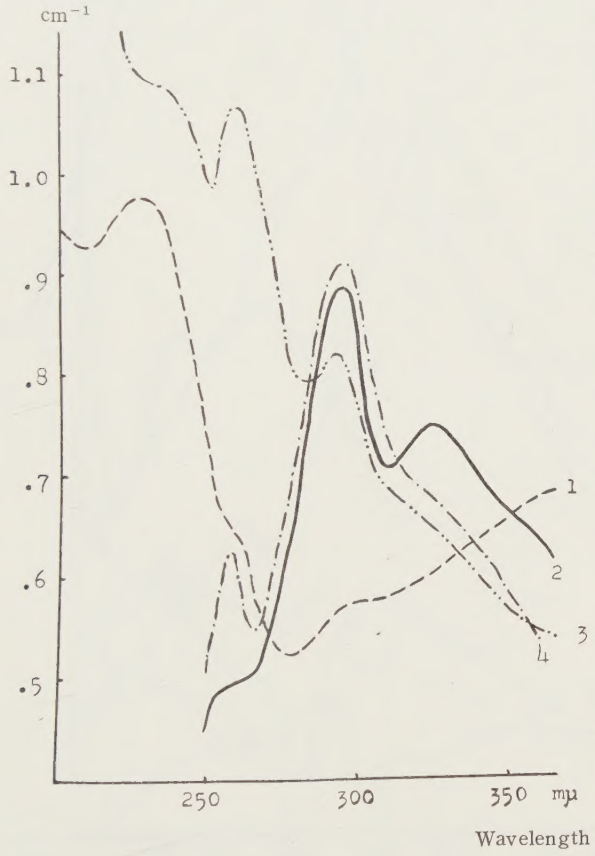

Fig. 2. Absorption bands of coloured NaCl
1. X-rayed
2. K-coloured in vacuum
3. F-coloured in vacuum
4. K-coloured in air

When brought up to 500°C, W-band became destroyed, separated with K-band and vanished at last. When the coloured NaCl crystal was brought up to 200°~250°C, R→K, K_2 and K′ transformation occurred, but in this case, W-band did not change.

The nature of W-band may be quite different from that of known bands in coloured alkali-halide crystals. So, we think, that is colloids of Na atoms.

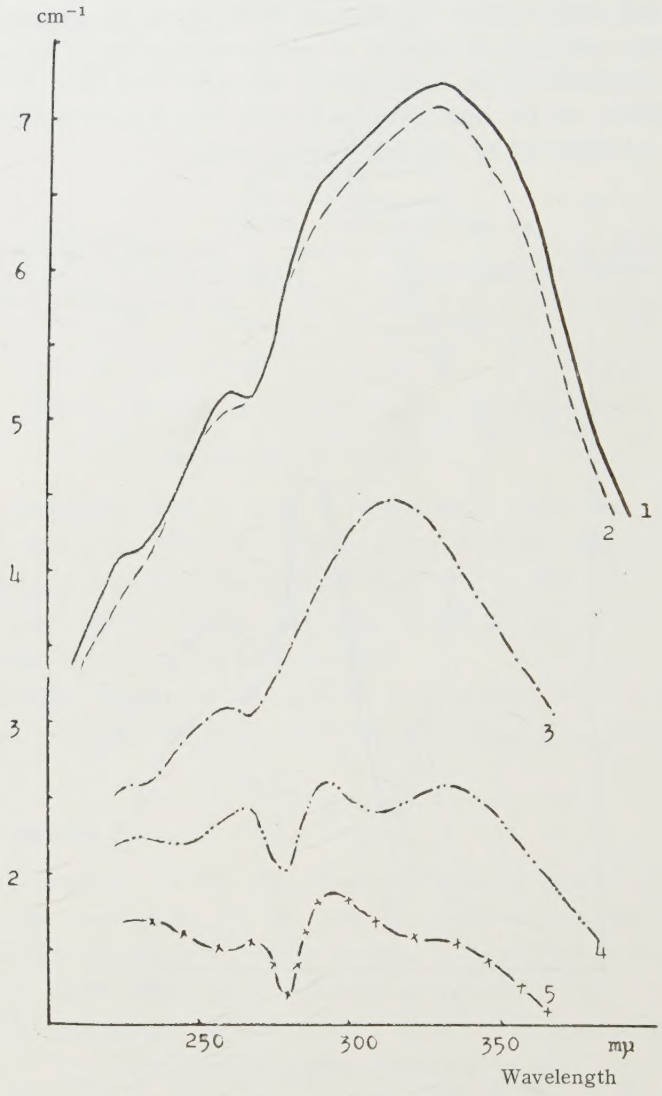

Fig. 3a. W-band of NaCl
1. K-coloured in vacuum
2. Exposed to K-light for 3.5 hours
3. Heated at 500°C for 3 hours
4. Heated at 550°C for 2 hours or more
5. Heated at 500°C for 2 hours or more

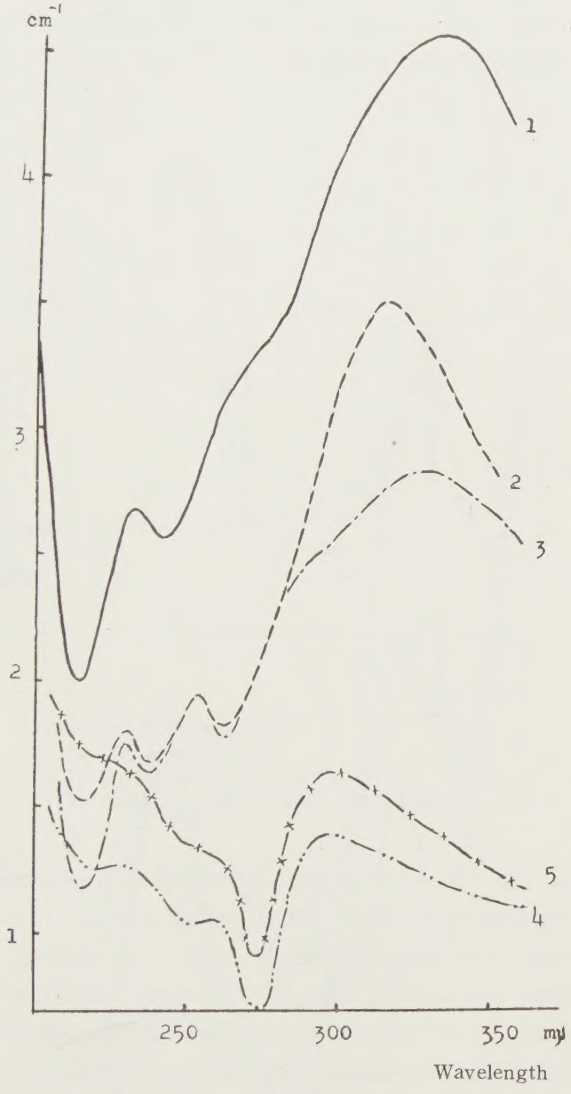

Fig. 3b. W-band of NaCl

1. K-coloured in vacuum
2. Heated at 500°C for 3 hours
3. Exposed to K-light for 1 hour
4. Heated at 500°C for 7 hours or more
5. Heated at 180°C for 4 hours or more

B. *K_2-band*

K_2-band appears in the crystals K-coloured at relatively low temperature or rapidly cooled after electrolysis. When brought up to 500°C, K- and K_2-bands were destroyed, and K_2-band was destroyed more easily than in the case of K-band. U-band on the

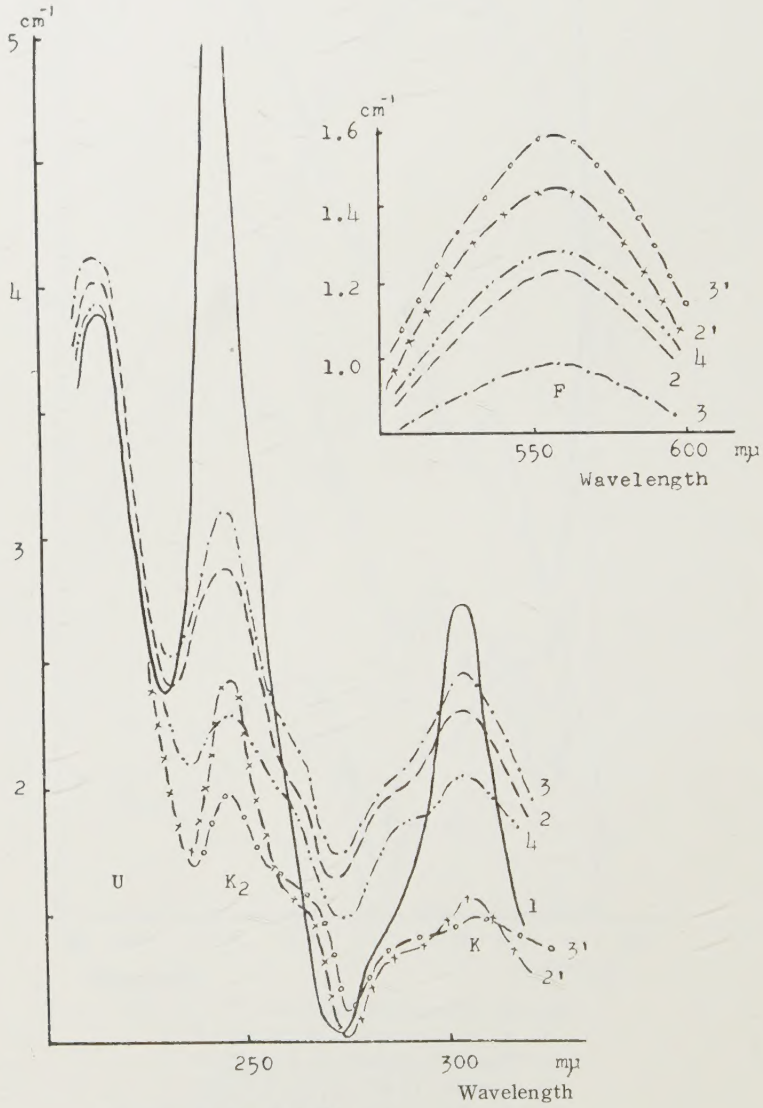

Fig. 4a. K_2-band of KCl
1. K-coloured in air
2. Bleached with K_2-light for 2.5 hours
3. Bleached with F-light for 2 hours or more
4. Bleached with K_2-light for 2 hours or more
2′. Bleached with K_2-light for 3 hours
3′. Bleached with K-light for 2 hours or more

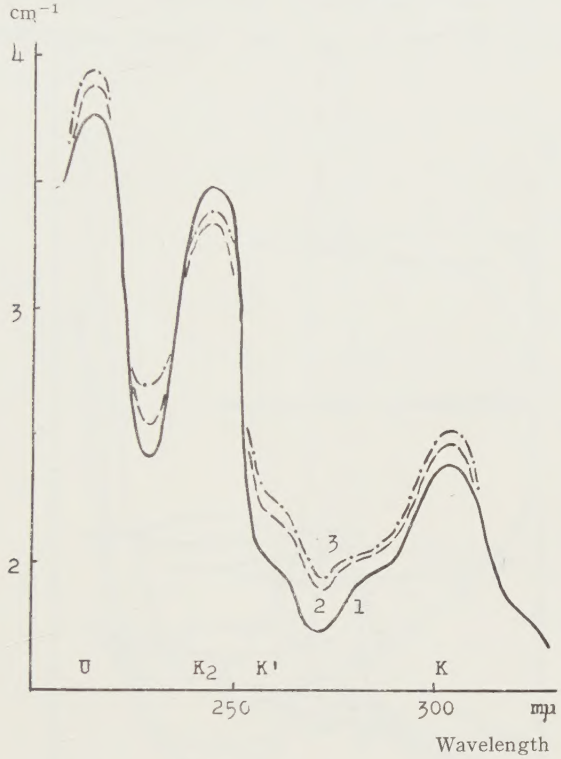

Fig. 4b. K_2-band of KCl
1. K-coloured in air
2. In the dark for a week
3. Bleached with R-light for 2.5 hours

side of shorter wavelength than K_2-band did not change. So this band is weak for the thermal treatment and so this band may not be found in past coloration.

By exposure to K_2-light or K-light, K-and K_2-bands were reduced and F-band was enhanced (Fig. 4-a). By exposure to F-light, F-band was reduced and K-, K_2- and K′-bands were enhanced. By exposure to R-light, K-, K_2- and K′-bands were enhanced. In these photo-transformations, the amount of transformation of K_2-band is larger than that of K-band.

When the coloured KCl crystal was brought up to 200°～230°C, R-band was destroyed and K-, K_2- and K′-bands were enhanced.

The nature of K_2-band is similar to K-band, except the weakness for thermal treatment.

C. *Crystals exposed to X-rays*

When the KCl crystals are exposed to X-ray, in the ultra-violet region, V-band

appears remarkably at room temperature. But when exposed to X-ray at high temperature (~ 300°C), W-, K-, K_2-, K′ and V-bands also appear as shown in Fig. 5.

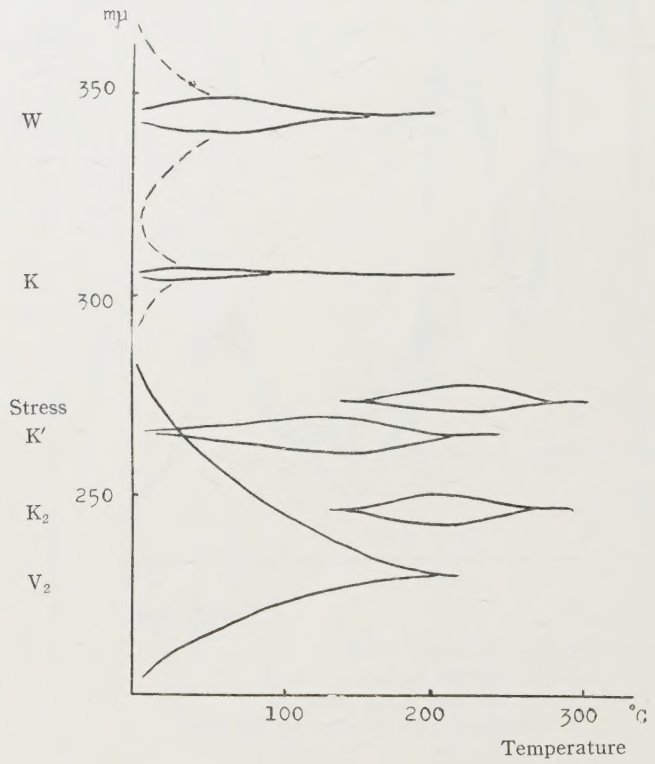

Fig. 5. Location of absorption bands of X-rayed KCl

D. *Stress-band*

When the KCl crystal was brought up to 500°C and rapidly cooled or subject to normal electrolysis for a short time, a new absorption band appeared in 275.5 mμ, and its absorption coefficient was about 0.2 cm^{-1}. When brought up to 500°C and subjected to electrolysis using iron string as anode and platinum plate as cathode, this band also appeared strongly and its absorption coefficient amounted to 1.5 cm^{-1}.

By exposure to the light lying in this band, this band did not change. When brought up to 500°C and slowly cooled, this band vanished, and this heat treatment is reversible.

This band also appears in the crystal exposed to X-ray heating up to 200°C.

The nature of this band may be in accordance with the stress growing in the crystal lattice. So this is called stress-band.

Fig. 6. 275.5 mμ stress band of KCl
1. Heated at 480°C for 2 hours and cooled rapidly
2. Heated at 500°C for 4 hours or more and cooled slowly
3. Heated at 500°C for 2 hours or more and cooled rapidly
4. Heated at 500°C for 2 hours or more and cooled slowly
5. Subjecting crystal to electrolysis and cooling rapidly

4. Discussion

When growing W-band, the crystal had to be slowly cooled in vacuum chamber after heating and its character was very different from other known bands. And so we wonder whether its nature can be colloids.

On the other hand, K_2-band is similar to K-band and its nature is the same one. But their energy states may be different on account of any element in the crystal. Hacskaylo mentioned in his paper that colour cloud in an electrolytically coloured crystal is removed either by reversing the polarity of the current or by continuing the flow of current in the same direction. These states are called metastable states.

Our K– and K_2–bands may appear in his metastable states. But, since these bands are different from stress-band, their nature may not be simple stress or deformation in crystal.

The writer wishes to express his cordial thanks to Professor Yôichi Uchida for his kind advices during the course of this work.

REFERENCES

1. H. Dorendolf: ZS. f. Phys., **129** (1951) 317.
2. Y. Uchida, M. Ueta and Y. Nakai: J. Phys. Soc. Japan, **6** (1951) 107.
   Y. Uchida and H. Yagi: J. Phys. Soc. Japan, **7** (1952) 109.
3. M. Hacskaylo and G. Groetzinger: Phys. Rev., **87** (1952) 789.
4. Y. Uchida and H. Yagi: J. App. Phys. Japan, **16** (1947) 65.
5. Y. Uchida and Y. Nakai: J. Phys. Soc. Japan, **9** (1954) 928.

Memoirs of the College of Science, University of Kyoto, Series A,
Vol. XXVII, No. 4, Article 2, 1956

SPECTRA OF COLOURED LITHIUM FLUORIDE CRYSTALS

BY

Yôichi UCHIDA and Hisao YAGI

(*Received March 1, 1956*)

ABSTRACT

Absorption bands of coloured lithium fluoride crystals in the wavelength regions between 1600～5500 Å were measured. These correspond respectively to K, F, R, M and N bands which were found in the absorption spectra of coloured alkali-chloride and alkali-bromide crystals.

1. Introduction

The analogy between the absorption spectra produced in coloured alkali-chloride and alkali-bromide is fairly clear and so corresponding bands in each of them can be classified as U, V, K, F, R, M and N. In the case of lithium fluoride, correspondence has not been so clear, but recently interesting results have been obtained by C. J. Delbecq and P. Pringsheim (**1**). This may be due to following reasons: Pure natural LiF crystals have not been obtained, but recently synthetic optical LiF crystals were made. The fact that the first fundamental absorption band lies below 1200 Å renders the studying for bands of shorter wavelength side than F-band quite hopeless without the use of vacuum spectrophotometer.

Fortunately, in our laboratory we succeeded in making LiF crystals by Kyropoulos' method. So we studied the absorption spectra of coloured LiF crystals using quartz and fluoride spectrophotometers.

2. Experimental procedures

Although visible accomplishments had not been remarkable, Slater (**2**), Kyropoulos (**3**), Ramsperger and Melvin (**4**), and Gyulai (**5**) had been sufficiently encouraging to warrant a continuation of LiF crystallization studies on a smaller scale. But, Stockbarger (**6**) succeeded in that work. In our laboratory, Kyropoulos' method (**7**) was employed.

$$Li_2CO_3 + 2HF \rightarrow LiF + CO_2 + H_2O \qquad (1)$$

At first, LiF powders were made from pure Li_2CO_3 by chemical reaction (1) and then LiF crystals were grown from these LiF powders.

In order to subject the crystals to electrolysis, they were mounted in a furnace

in a manner as shown in Fig. 1. A crystal was supported between two iron rods which served as a part of the electrical circuit supplying the current for electrolysis. The one rod (A) is sharply pointed at its end and acts as cathode. The other (B) contacts the crystal with the carbon plate covered with platinum foil and acts as anode. All parts except the furnace can be evacuated. Current is supplied by a 450 volt power supply with a 500 KΩ resistor.

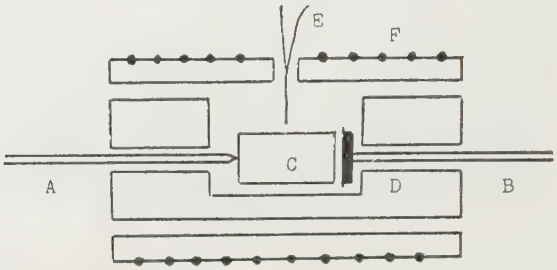

Fig. 1. Arrangement for subjecting crystals to electrolysis.
A : cathode, D : holder,
B : anode, E : thermocouple,
C : crystal, F : furnace.

After inserting a crystal in the furnace, the temperature of the furnace was first raised up to 450°~500°C, and the current was supplied, and colour cloud was made electrolytically in the crystal. (This coloured condition is called "F-coloured".) Then the temperature of the furnace was brought down to 350°~400°C, and the coloured cloud in the crystal was removed by reversing the polarity of the current. (This coloured condition is called "K-coloured".)

For the irradiation with X-rays, a Mazda Sealex tube, operated at a voltage of 30 KV D.C. and a current of 8 mA, was used. During the irradiation the crystal was kept in dark and at room temperature.

The crystals used were always freshly cleaved on all sides at the last possible moment before starting experiment.

The absorption spectra of the crystals were obtained with a quartz-prism spectrophotometer with 1 meter focal length objective. Monochromatic light from the second slit was measured photoelectrically by Sb-photocell made of quartz and a Dolezaleck quadrant electrometer (sensitivity: 1500 D/V) connected in the way as shown in Fig. 2. A CaF_2-prism vacuum spectrograph was used in the region between 2000 Å and 1500 Å and absorption spectra were obtained from the photographic plates by the recording microphotometer.

For the light source, a hydrogen discharge tube (6000 V, 1 A.) was used. RCA

photomultiplier tube 1P-28 was also used in place of the photocell. A Beckman Quartz Spectrophotometer Model DU was also used.

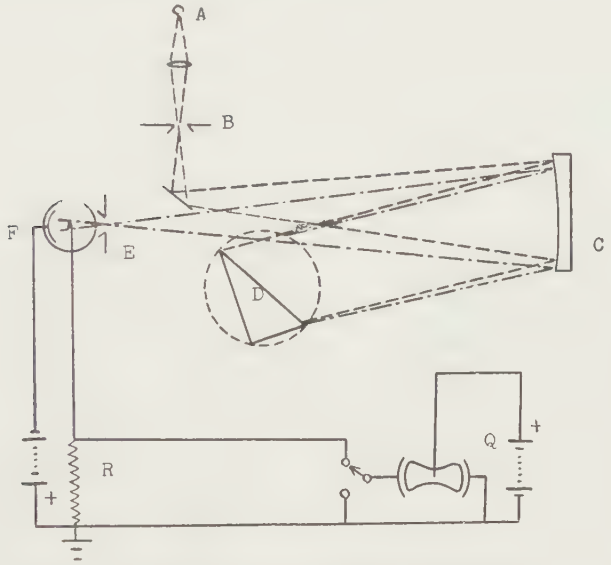

Fig. 2. Arrangement for measuring absorption.
A : light source, E : 2nd slit,
B : 1st slit, F : photocell,
C : collimator, mirror, R : 10^{10} ohms,
D : prism, Q : quadrant electrometer.

3. Results obtained

Absorption spectra of coloured LiF-crystal is shown in Fig. 3, and wavelengths of their band maxima are given in Table 1. Values of these bands agree with those obtained from Ivey's empirical formula (8)* which has been derived from the values of absorption bands of NaCl, KCl and KBr. Among these R-bands, a peculiar wave number relation is seen as follows:

$$\frac{\nu_\alpha - \nu_\beta}{\nu_\gamma - \nu_\delta} = \frac{\nu_\beta - \nu_\varepsilon}{\nu_\delta - \nu_\zeta} \quad \text{approximately.}$$

Our N-band corresponds to 520 mμ band found by Schneider (**9**) in LiF and near infra-red band in NaCl found by Molnar and in KCl and KBr by Oberly (**10**). Precise characters in N-band have not yet been known and only Petroff (**11**) reported that N-band appeared after M-band by exposure to F-light in KCl crystal.

---

* Ivey's empirical formula is given by

$$\lambda_{max} = Cd^x,$$

where λ_{max} is wavelength of absorption maximum of each band, d is the lattice constant of each crystal, C is a certain constant and x is a certain exponent. The latter two vary from band to band.

When K-coloured LiF crystal was irradiated by 546 mμ line of Hg lamp, N-band was reduced and F- and M-bands were enhanced as shown in Fig. 3. When this sample was measured while kept in dark room for two days, reduced band was

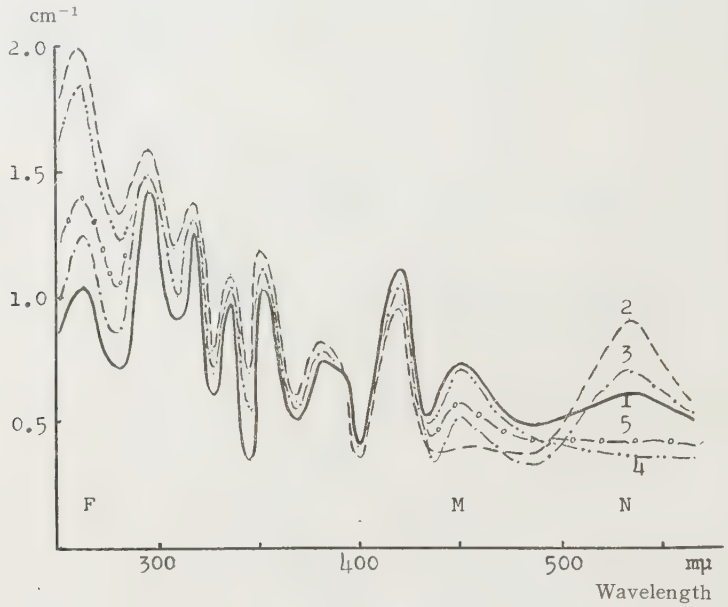

Fig. 3. Absorption bands of coloured LiF.
1. K-coloured
2. Bleached with Hg 465 mμ for 25 minutes
3. In the dark for 5 days
4. Bleached with Hg 546 mμ for 25 minutes
5. In the dark for 2 days

Table 1. Absorption bands of coloured LiF crystal.

Absorption bands	Wavelength in mμ	Energy in eV	Ivey's formula
N	530	2.33	$1950\ d^{1.40}$
M	468	2.63	$1780\ d^{1.36}$
R_α	408	3.02	$1330\ d^{1.55}$
R_β	377	3.27	$1260\ d^{1.54}$
R_γ	355	3.47	$1230\ d^{1.53}$
R_δ	338	3.65	$1170\ d^{1.54}$
R_ε	315	3.91	$1120\ d^{1.54}$
R_ζ	297	4.15	$1070\ d^{1.54}$
F	270	4.57	$724\ d^{1.80}$
K	183	6.75	
K′	161	7.66	

These results were obtained at room temperature.

enhanced and enhanced bands were reduced and thermal equilibrium was accomplished. In this light bleaching, R-band did not change.

When irradiated by 435 mμ line of Hg lamp, M-band was reduced and F-, R- and N-bands were enhanced and the thermal equilibrium was obtained after three days. When M- and N-bands were bleached, relations of photo-transformation vs. time among various centres were shown in Tables 2 and 3. Numerical values in these tables are for $[(\kappa-\kappa_0)/\kappa_0]\times 100$, where κ_0 is the initial absorption coefficient and κ the absorption coefficient after bleaching.

Table 2. M-bleaching in LiF.

Bleaching time in minutes	Bands			
	F	Rβ	M	N
3	8	10	−20	90
5	6	7	−25	80
10	4	4	−28	60
20	2	1	−30	44
30	2	0	−32	44

Table 3. N-bleaching in LiF.

Bleaching time in minutes	Bands			
	F	R	M	N
3	5	0	20	−30
5	1	0	15	−40
10	−0.5	0	10	−50
20	−1	0	10	−55
30	−3	0	10	−60

When irradiated by the light of Hg lamp through Mazda UV-D1 filter (just lying in R-band) F- and M-bands were enhanced and N-band did not change.

By exposure to 185 mμ line of Hg lamp (just lying in K-band), F- and R-bands were enhanced as shown in Table 4.

Table 4. K-bleaching in LiF.
(unit: cm^{-1})

Bands	F	Rα	Rβ	Rγ
Initial absorption	3.2440	1.9655	1.7620	2.2630
difference	+1.5	+0.5	+0.71	+1.9
Bleached for 5 hours	4.700	2.4305	2.4715	4.1050
difference	−0.3	−0.3	−0.3	−0.9
After 16 hours	4.4630	2.1450	2.1150	3.2220

Table 5. K′-bleaching in LiF.
(unit: cm^{-1})

Band	F
Initial absorption	1.5940
difference	+0.96
Bleached for 5 hours	2.5540
difference	−0.06
After 16 hours	2.4145

By exposure to 165 mμ of H_2 discharge tube using vacuum spectrograph, F-band was enhanced as shown in Table 5.

Correspondence among the absorption spectra produced in coloured alkali-chloride, alkali-bromide and alkali-fluoride becomes fairly clear in these experiments. Precise investigation for each band has not yet been done, but it may be very interesting.

REFERENCES

1. C. J. DELBECQ and P. PRINGSHEIM: J. Chem. Phys., **21** (1953) 794.
2. SLATOR: Proc. Am. Acad., **61** (1925) 136.
3. S. KYROPOULOS: ZS. f. anorg. u. allgem. Chemie, **154** (1926) 308.
4. RAMSPERGER and MELVIN: J. Opt. Soc. Am., **15** (1927) 359.
5. GYULAI: ZS. f. Phys., **46** (1928) 80.
6. D. C. STOCKBARGER: Rev. Sci. Inst., **7** (1936) 133.
7. Y. UCHIDA and H. YAGI: J. App. Phys. Japan, **16** (1947) 65.
8. H. IVEY: Phys. Rev., **72** (1947) 341.
9. E. G. SCHNEIDER: J. Opt. Soc. Am., **27** (1937) 72.
10. J. J. OBERLY and E. BURSTEIN: Phys. Rev., 76 (1949) 1254, and Am. Phys. Soc. Washington, April 28, (1950).
11. S. PETROFF: ZS. f. Phys., **127** (1950) 443.

MEMOIRS OF THE COLLEGE OF SCIENCE, University of Kyoto, Series A,
Vol. XXVII, No. 4, Article 3, 1956

ON THE EARTH'S MANTLE

BY

Haruo MIKI

(*Received March 15, 1956*)

1. Introduction (1)

The interior of the earth is one of the attractive problems of popular interests and many studies have been done on it from old times, as well as on the origin of the magnetic main field of the earth, but we have only a few established facts. There is no lack of informations—astronomical, geochemical, petrological, geological, geophysical—but the relationships of most of these materials to the earth's interior are vague. The values of seismic velocities at definite depths of the earth's interior derived from seismology are important in the sense that they are concerned with the interior directly. The information, however, has an abstract character and the chief efforts of the theory to the internal constitution of the earth have been directed to decipher this information. It is needless to say that the conclusions we have reached reflect uncertainties which are still present in the seismological data, as well as in our knowledges of the materials. Since the discussion is largely based on an analysis of details of the variations with depth of the velocities of two seismic waves, we commence with some preliminary remarks upon the reliabilities of these velocities.

1.1. Distributions of velocities of seismic waves within the earth

The curves of velocity *versus* depth (or radius), which we are handling in special, can be found by processes of integrations of the travel-time curves, which embody the observations most directly. But, it is not always easy to obtain the objective validity of the travel-time curve, i.e., it depends upon the discriminations of the various phases of a seismogram, the choice of materials (seismograms of the same earthquake recorded at the same station do not always coincide on account of the differences of constants in seismometers), the construction of travel-time curves (the least square approximation can lessen the error) and etc. (2). There is a method of Wiechert-Helglotz to obtain the values of seismic velocities from the travel-time curves in the deeper part of the earth, but this method cannot be applied to the part shallower than the depth of some ten kilometers. In addition to the above difficulties, the local characteristics of the crust make it more difficult to obtain the values of seismic velocities. The distributions of seismic velocities employed by us at present are

obtained after the efforts tiding over these difficulties and lessening the errors as far as possible.

On the one hand, disagreements among seismologists exist with respect to a number of features of the velocity-depth curves, but on the other hand, the agreement with regard to the major characteristics of these curves is being confirmed, and revision which would invalidate a serious portion of the following analysis seems unlikely. The velocity-depth curves of both Jeffreys (**3**) and Gutenberg (**4**) are plotted in Fig. 1.

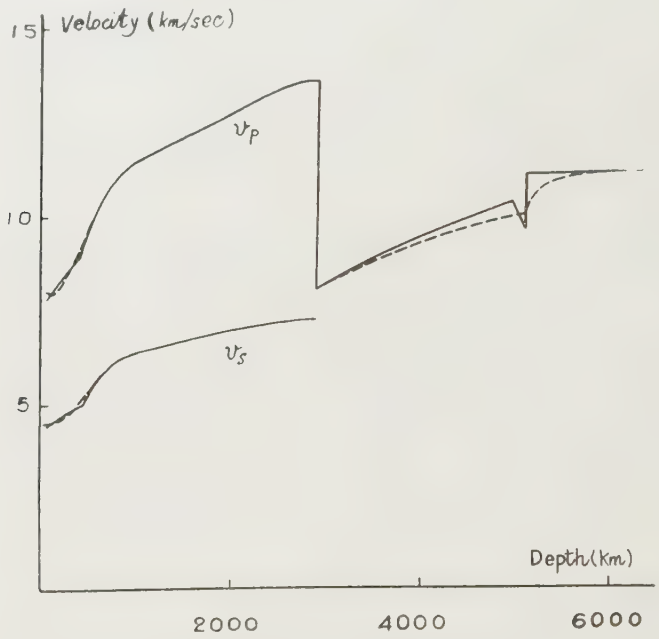

Fig. 1. Velocity-depth curve.
—— after Jeffreys, ····· after Gutenberg.

1.2. Outline of the density distribution within the earth

Until some 50 years ago, the principal sources of information about the earth's interior were geodesy and astronomy. The mean density and moment of inertia were known, and there were estimates of the effective rigidity based on the study of earth tides. Since the mean density was about 5.5 gr/cm^3, as compared with values usually less than 3 gr/cm^3 for surface rocks, and the moment of inertia was about $\frac{1}{3}MR^2$, as compared with $\frac{2}{5}MR^2$ for a sphere of uniform density, it has long been clear that there must be an increase of density towards the centre; these two pieces of informations just determined such two-parameter relations between density and radius as those of Laplace and of Roche. It was calculated by Kelvin that the effective

rigidity was somewhat greater than that of steel and the result was in conflict with the prevailing geological concept of his day, because the earth was thought to be a generally liquid globe covered by a thin crystalline "crust".

The first calculation based on a definite physical picture of the interior seems to be that of Wiechert. He divided the interior into uniform two parts, central sphere of iron and a shell composed of heavy silicates. This subdivision was suggested by the most striking fact about meteorities, that they are chiefly composed of the distinctly different materials, silicates and metallic iron. Iron is the most abundant of the heavy elements, not only in surface rocks and meteorites, but also in the outer layers of the sun and other stars; its existence in the meteorites as free metal gives a definite suggestion for a metallic core in the earth.

With the development of instrumental seismology, facts began to accumulate regarding definite levels inside the earth. The central core postulated by Wiechert was now discovered to have physical reality, though its size, as determined later by Gutenberg, was very different from that of Wiechert's core. It was remarked by L. H. Adams and E. D. Williamson (5) that the seismic velocities could be used to obtain the change of density with depth and to improve the rough suggestion after Wiechert.

The Adams-Williamson equation is as follows: The ratio of incompressiblility K_S to density ρ for an isotropic elastic body is

$$\frac{K_S}{\rho} = \phi = \left(\frac{\partial P}{\partial \rho}\right)_S = v_p^2 - \frac{4}{3} v_s^2 , \tag{1.1}$$

where P is the pressure, S entropy, v_p, v_s seismic velocities of longitudinal and transversal waves, respectively, and ϕ convenient notation for K_s/ρ introduced by Bullen. ϕ can be expressed as a function of radius from the earth's centre by means of (1.1), because the values of seismic velocities, v_p, v_s, are known. We assume that the change of pressure is given by the hydrostatic relation, $dP = -g\rho\, dr$. Then, if the change of density is based on the adiabatic compression alone, we have the Williamson-Adams relation:

$$\frac{d\rho}{\rho} = -g(r)\frac{dr}{\phi(r)} , \tag{1.2}$$

where $g(r)$ is the acceleration of gravity and is expressed as follows:

$$\begin{aligned} &g(r) = G\frac{M(r)}{r^2} , \quad M(r) = 4\pi\int_0^r \rho r^2\, dr , \\ &G = 6.670 \times 10^{-8} \text{ dynes. cm}^2/\text{gr.} \end{aligned} \tag{1.3}$$

Numerical integration of this equation leads us to the change of density within any layer satisfying the assumption of homogeneity and adiabaticity; the absolute density

must be adjusted to satisfy conditions for the mass and moment of inertia. In the case of the earth, these values are

$$M(a) = 58.97 \times 10^{26} \text{ gr},$$
$$I(a) = 79.14 \times 10^{43} \text{ gr. cm}^2.$$

This procedure, originally carried through by Williamson and Adams, has been repeated by Bullen with more recent data, in a series of important papers (**6**).

Bullen assumed that the density change in the C layer (413～984 km) was quadratic on account of the gradual changes of chemical composition and lattice structure proposed for this layer by Bernal (**7**) and Jeffreys (**8**). After some unimportant simplifications, he calculated the density distribution, using these assumptions and the method essentially equivalent to that of Williamson and Adams. The pressure distribution can be obtained by means of the density distribution and hydrostatic relation assuming the small initial pressure at the depth of 33 km.

Table 1.1 Bullen's distribution of density and pressure, and the corresponding temperature (**9**).

Depth (km)	Density (gr/cm^3)	Pressure (dyne/cm^2)	Temperature (°K)
33	3.32	0.009×10^{12}	T_1
100	3.38	0.031	$1.030\,T_1$
200	3.47	0.065	$1.075\,T_1$
300	3.55	0.100	$1.125\,T_1$
413	3.64	0.141	$1.181\,T_1$
500	3.88		
600	4.11	0.213	
800	4.46	0.300	
1000	4.65	0.392	T_2
1200	4.88	0.58	$1.030\,T_2$
1800	5.10	0.78	$1.055\,T_2$
2200	5.31	0.99	$1.077\,T_2$
2600	5.51	1.20	$1.098\,T_2$
2898	5.66	1.37	
2898	9.7		
3000	9.9	1.47	
3500	10.5		
4000	11.1	2.40	
4500	11.6		
4982	11.9	3.17	
5121	12.0		
6371	12.3		

1.3. Remarks on the method of Williamson-Adams-Bullen

Bullen's distributions seem to be plausible at first sight, but they are based on the various assumptions not yet proved to be valid. Namely, the quadratic distribution of density in the C layer is not an established fact and there is no reason that the following conditions

homogeneity
adiabatic temperature gradient
hydrostatic equilibrium

are satisfied in the other layers of the mantle. But, this distribution of density is convenient to know the rough features of the distributions of density and pressure inside the earth. Then, let us examine Williamson-Adams-Bullen's method to avoid the deficiency of this method.

The change of density with radius may be written in terms of coefficients of isothermal incompressibility K_T and thermal expansion α,

$$\frac{d\rho}{dr}=\left(\frac{\partial\rho}{\partial P}\right)_T\frac{dP}{dr}+\left(\frac{\partial\rho}{\partial T}\right)_P\frac{dT}{dr}=-\frac{g\rho^2}{K_T}-\rho\alpha\frac{dT}{dr}. \tag{1.4}$$

In general,

$$\frac{dT}{dr}=\frac{T\alpha V}{C_p}\frac{dP}{dr}-\tau=\frac{T\alpha gA}{C_p}-\tau, \tag{1.5}$$

where C_p is specific heat at constant pressure per mole and A is mean atomic weight, the gradient of temperature τ merely denoting the difference between the actual gradient of temperature and the adiabatic gradient, $-T\alpha gA/C_p$ (the negative sign arising from differentiation with respect to radius instead of depth). By virtue of the thermodynamic relations between isothermal incompressibility K_T and adiabatic incompressibility K_S,

$$\frac{K_T}{K_S}=1-\frac{T\alpha^2VK_T}{C_P}, \tag{1.6}$$

the equation for density change may be written

$$\frac{d\rho}{dr}=-\frac{g\rho^2}{K_S}+\alpha\rho\tau=-\frac{g\rho}{\phi}+\alpha\rho\tau. \tag{1.7}$$

The term in τ is neglected in Williamson-Adams' method, but it may be appreciable. If we assume $\alpha\approx2\sim3\times10^{-5}$ deg^{-1}, $\rho\approx4\sim5$ gr/cm^3, $\tau\approx1\sim2$ deg/km, we find $\alpha\rho\tau\approx1\sim3\times10^{-4}$ gr/cm^3. km. Therefore, the method of Williamson-Adams yields error of about $0.1\sim0.3$ gr/cm^3 per 1,000 km, and this error increases and is accumulated in the process of numerical integration. The error with this order of magnitude is appreciable in the calculation performed by use of the density distribution.

Let us calculate the adiabatic temperature gradient (**10**) assumed by Williamson, Adams and Bullen. From (1.5) the adiabatic temperature gradient is given by

$$\frac{d\log T}{dr}=-\frac{\alpha g A}{C_P}, \tag{1.8}$$

and we find

$$\frac{d\log T}{dr}=-\frac{\gamma_G}{\phi}g, \tag{1.9}$$

by means of the following relation in chemical physics (**11**), namely:

$$\gamma_G=\frac{\phi\alpha A}{C_P}, \quad (\gamma_G: \text{ Grüneisen's ratio}). \tag{1.10}$$

Since

$$\gamma_G=\frac{\partial\log\nu_m}{\partial\log\rho}, \tag{1.11}$$

where ν_m is Debye's maximum frequency given by

$$\nu_m=\left(\frac{9}{4\pi}\frac{N}{A}\frac{\rho}{v_p^{-3}+2v_s^{-3}}\right)^{1/3}, \tag{1.12}$$

the distribution of γ_G within the earth can be estimated by means of the distribution of seismic velocities and Bullen's density. The temperature distribution corresponding to Bullen's density distribution can be estimated by means of (1.9) and the distribution of γ_G estimated as above (see Table 1.1). We have excluded the C layer from the calculation, because it is not clear whether his distribution satisfies the condition of homogeneity in this layer. We see in Table 1.1 that the increase of temperature is very small, i.e., if we take $T_1=1{,}000°K$ and $T_2=2{,}000°K$, the increase of temperature in the B layer (33～413 km) and the D layer (984～2898 km) amount to only about 180° and 200° respectively.

1.4. Division of the earth

The object of the study of the earth's *interior* has been the earth's model stripping the "crust". There is no important reason to consider the earth's model stripping the "crust", it seems only to be one of the customs in this branch of science. This custom probably depends upon the following conveniences:

(a) The "crust" has very complicated structure (involving horizontal inhomogeneity).

(b) The mass and the moment of inertia of the earth are not seriously affected by the crust stripped, since the density and the volume of the crust is small in comparison with the whole earth.

(c) The assumption of hydrostatic equilibrium is convenient for the theoretical treatment, but probably this assumption is not satisfied in the "crust".

The characteristic of this "crust" is in the low seismic velocities, compared with the high values of deeper part of the earth. The bottom of the crust should not be equal all over the earth, but it has been customarily drawn at the depth of 33 km. This depth corresponds to that of the Mohorovicic discontinuity under European continent. The structure of the crust does not affect directly the various properties of the earth's interior, but affect seriously the determinations of the seismic velocities, on which most of the discussions on the earth's interior depend, for the seismic velocities are small in that part. Recently, the determination of fine structure of the crust is being tried at some places in the world by means of the artificial earthquake. Since the exact knowledge about the crust is one of the keys for the determinations of seismic velocities, the result derived by the artificial earthquake cannot be neglected in the theory of the internal constitution of the earth. There must be local (horizontal) differences in the distributions of seismic velocities, but these localities would decrease with increasing depth or be involved in the error which increases with depth. Therefore, we consider the ideal earth by use of the seismic data with no local difference.

Seismologists now recognize some half-dozen subdivision of the interior of the earth. Although complete identification with the interior itself as for the boundaries of these divisions, or even the existence of some of them, had not been reached, it is convenient to have designations for them, and at least rough indications of their positions and relative volumes and masses. The figure of Table 1.2 follows Bullen (**9**), where layers are based on Jeffreys' solution for the velocity-depth relations.

Table 1.2 Dimensions and masses of the internal layers. (after Bullen (**9**))

Layer		Depth to boundaries	Fraction of volume	Fraction of total mass
		0 km		
Crust	A	33	0.0155	0.008
Mantle	B	413	0.1665	0.104
	C	984	0.2131	0.164
	D	2898	0.4428	0.410
Core	E	4982	0.1516	0.315
	F	5121	0.0028	
	G	6371	0.0076	

2. C-layer

The seismic velocities increase with increasing depth as shown in 1.1, but the variations of seismic velocities in the upper mantle and the C layer are noteworthy. Especially, the C layer plays an important role for the determinations of distributions of density and pressure, i.e., the interpretation about the physical properties of the C layer has the influence on the determinations of physical properties in other layers, because these determinations are usually performed by the numerical integrations. Besides the above theoretical importance, the interest for the C layer has recently been raised more and more on account of the seismic facts that the deep focus earthquakes occur down to the C layer and probably do not occur in the deeper part (**12**). Perhaps it is not wrong that almost all the important problems about the mantle cannot be solved without the elucidation of C layer and that the C layer is the key to solve the question about the mantle.

Unless otherwise noted, the values of seismic velocities due to Bullen (**9**) are adopted in numerical culculations.

2.1. Characteristics of C-layer

The distribution of $\phi=K_S/\rho$, Poisson's ratio σ and K_S/μ in the earth's mantle can be obtained by means of the values of seismic velocities (Fig. 2.1). The abnormal changes of these quantities in the C layer, compared with other layers, are found in Fig. 2.1. In order to make clear these abnormal changes of elasticities in the C layer, various attempts have been done as follows :

(a) Case when the earth's mantle is homogeneous, isothermal and is in the state of hydrostatic equilibrium (**13**)

By means of the following equations :

$$dP=-g\rho\,dr\,, \qquad \text{(from the assumption of hydrostatic equilibrium)} \tag{2.1}$$

$$P=3K_0f(1+2f)^{5/2}\,, \tag{2.2}$$

$$\rho=\rho_0(1+2f)^{3/2}\,, \qquad \text{(from the theory of finite strain)} \tag{2.3}$$

we find

$$h-h_0=\frac{3\lambda+2\mu}{g\rho_0}\left[f\left(1+\frac{7}{2}f\right)-f_0\left(1+\frac{7}{2}f_0\right)\right], \tag{2.4}$$

where K_0 is the bulk modulus at zero pressure, f the negative strain and λ, μ Lamé constants.

The density distribution can be obtained by means of (2.3) and (2.4), since the acceleration of gravity g is nearly constant throughout the mantle.

The relations between the negative strain and the velocities of elastic waves are

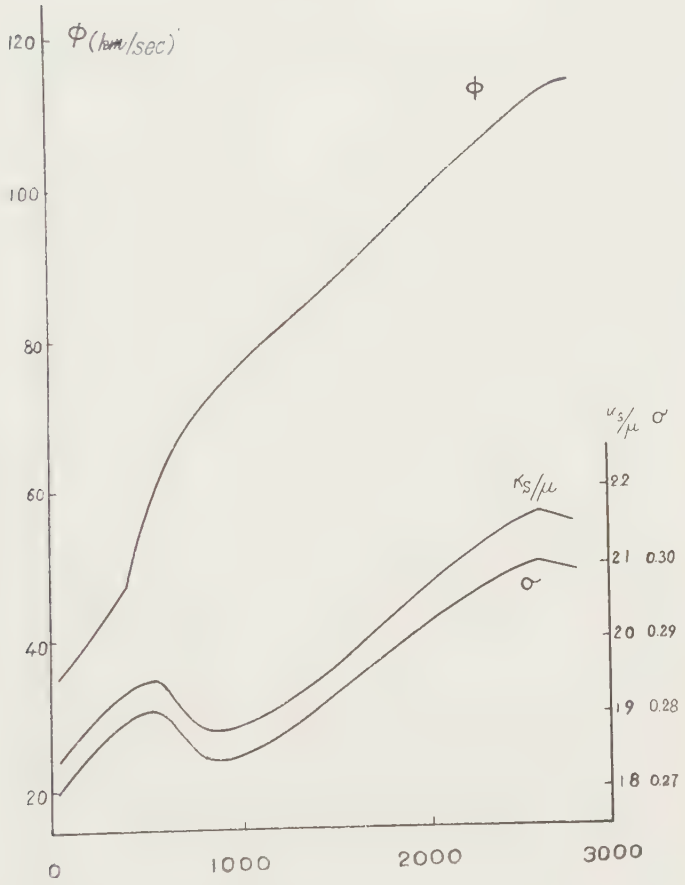

Fig. 2.1 Distribution of $\phi=K_S/\rho$, Poisson's ratio σ and K_S/μ.

$$v_p^2=v_{p0}^2(1+2f)\left\{1+f\frac{11m+10}{m+2}\right\}, \tag{2.5}$$

$$v_s^2=v_{s0}^2(1+2f)\{1+f(3m+4)\}, \tag{2.6}$$

with $$m=\frac{v_{p0}^2}{v_{s0}^2}-2,$$

v_{p0}, v_{s0} being the velocities of elastic longitudinal and transversal waves at zero pressure, respectively.

The distributions of seismic velocities can be estimated by means of (2.4), (2.5) and (2.6). In 1939 Birch calculated the distributions of density and seismic velocities, assuming the following initial values:

$$\rho_0=3.28 \text{ gr/cm}^3,$$
$$v_{p0}=7.6 \text{ km/sec}, \quad v_{s0}=4.3 \text{ km/sec}.$$

But he was obliged to assume the following initial values in order to suit them to the observed data in the D layer, though these are too high for ordinary rocks,

$$\rho_0 = 3.92 \text{ gr/cm}^3,$$
$$v_{p_0} = 8.75 \text{ km/sec}, \quad v_{s_0} = 4.77 \text{ km/sec}.$$

The results of calculations are shown in Fig. 2.2 and Fig. 2.3. The agreements with the observed values are fairly good except the C layer.

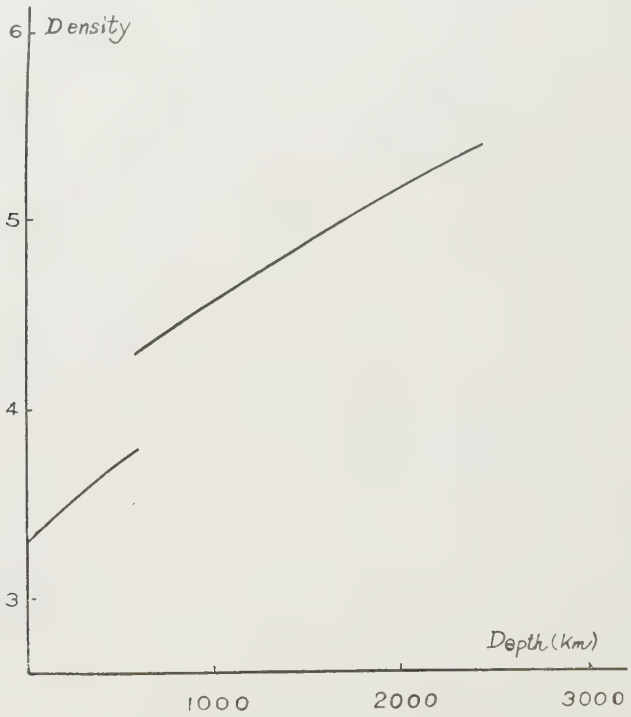

Fig. 2.2 Density distribution after Birch.

(*b*) *Case when the earth's mantle is homogeneous, in the state of hydrostatic equilibrium and has the adiabatic temperature gradient*

(1) The density distribution can be obtained by integrating Williamson-Adams' equation:

$$\frac{d\rho}{\rho} = -g(r)\frac{dr}{\phi(r)}, \quad \phi(r) = \frac{K_S}{\rho} = v_p^2 - \frac{4}{3}v_s^2, \tag{2.7}$$

$$g(r) = G\frac{M(r)}{r^2}, \quad M(r) = 4\pi\int_0^r \rho r^2 dr, \tag{2.8}$$

$$G = 6.670 \times 10^{-8} \text{ dynes. cm}^2/\text{gr}.$$

But the initial density should not be taken arbitrarily. The relation between initial

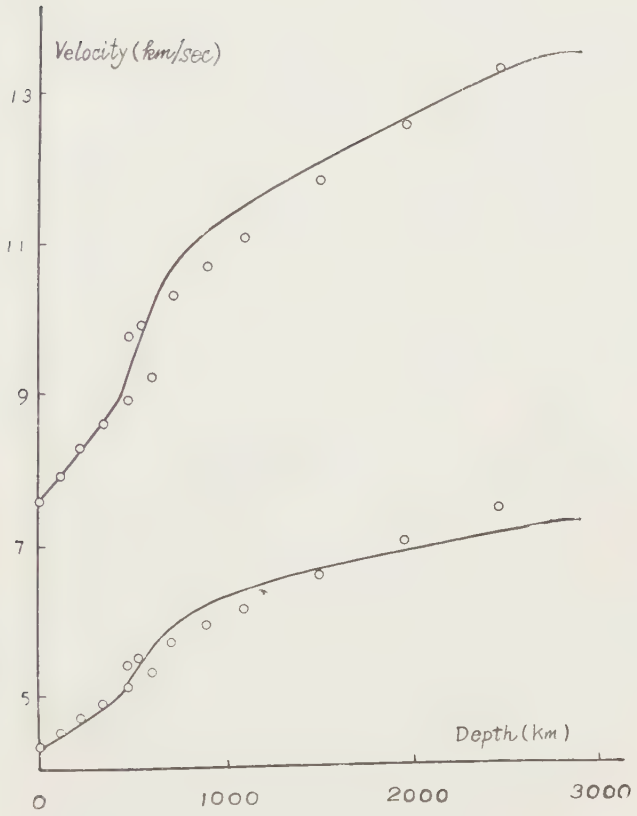

Fig. 2.3 Distribution of velocities of seismic waves after Birch. Solid lines show the observed values.

density and I/MR^2 which must be attributed to the earth's core is shown in Fig. 2.4. It is reasonable to assume that the density increases with increasing depth in the earth's core. Therefore, $I/MR^2<0.4$ and we see from Fig. 2.4 that the initial density must be greater than 3.7 (**12**). But ordinary minerals do not have such a high density at the pressure of about 10,000 atm. and temperature of about some hundred degrees.

(2) The ratio of adiabatic incompressibility K_S to isothermal one K_T is

$$\frac{K_S}{K_T}=1+T\alpha\gamma_G\,, \tag{2.9}$$

and the ratio of isothermal incompressibility to density is

$$\frac{K_T}{\rho}=\left(\frac{K_T}{\rho}\right)_0(1+2f)(1+7f)\,, \tag{2.10}$$

where $(K_T/\rho)_0$ is the zero-pressure value of K_T/ρ. Then, we find

$$gdh=K_S\frac{d\rho}{\rho^2}=\left(\frac{3K_T}{\rho}\right)_0(1+7f)df(1+T\alpha\gamma_G)\,, \tag{2.11}$$

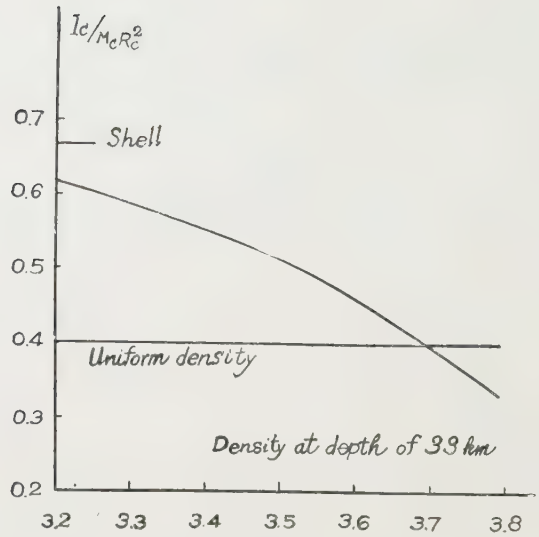

Fig. 2.4 Relation between $I_C/M_CR_C^2$ and the density at depth of 33 km.

by means of (2.3), (2.7), (2.9) and (2.10). $1+T\alpha\gamma_G$ is close to unity and taking a mean value of this quantity and integrating (2.11), we obtain

$$g(h-h_0)\approx\left(\frac{3K_T}{\rho}\right)_0 f(1+3.5f)\,\overline{(1+T\alpha\gamma_G)}$$
$$\approx 3\phi_0 f(1+3.5f)\,, \qquad \text{approximately.} \tag{2.12}$$

Again, making use of (2.10), we find

$$\frac{g(h-h_0)}{3\phi}\approx\frac{f(1+3.5f)}{(1+2f)(1+7f)}\,, \qquad \text{approximately.} \tag{2.13}$$

Since ϕ can be known as a function of depth by means of the seismic velocities, the relation between f and h can be obtained from (2.13), assuming g to be constant throughout the earth's mantle. Then the relation between ϕ_0 and h is found by means of (2.12) (Fig. 2.5). If the earth's mantle is homogeneous, in the state of hydrostatic equilibrium and has the adiabatic temperature gradient, ϕ_0 should be constant throughout the mantle. Fig. 2.5 conflicts with this expectation.

The above considerations on the distributions of density, seismic velocities, ϕ_0 and the initial density show that the following conditions

homogeneity
adiabaticity (approximately equals to isothermal condition)
hydrostatic equilibrium

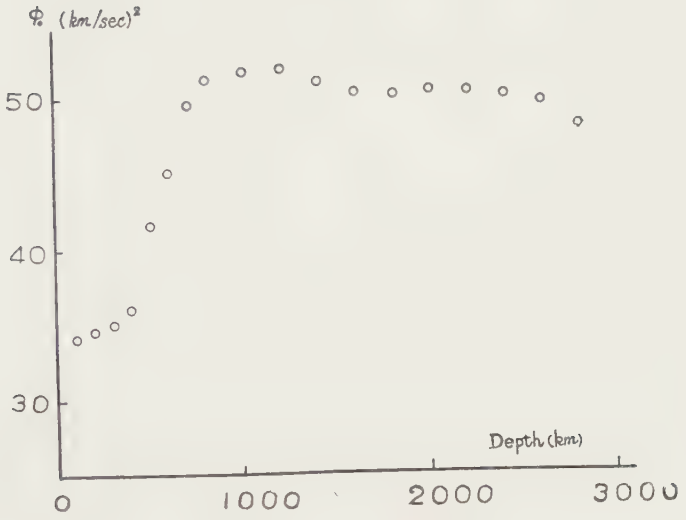

Fig. 2.5 Distribution of ϕ_0.

are not satisfied simultaneously in the mantle, especially in the C layer.

If we assume that the earth's mantle is homogeneous and in the state of hydrostatic equilibrium, having no touch on the temperature distribution, $1-g^{-1}d\phi/dr$, the quantity pointed out by Bullen (**14**), can be expressed as follows (**1**):

$$1-g^{-1}\frac{d\phi}{dr}=\left(\frac{\partial K_T}{\partial P}\right)_T-5T\alpha\gamma_G-2\frac{\tau\alpha\phi}{g}. \tag{2.14}$$

On the other hand, the change of Grüneisen's ratio γ_G, thermal expansion α and $(\partial K_T/\partial P)_T$ with negative strain are shown in Table 2.1.

Table 2.1 Estimation of Grüneisen's ratio, thermal expansion and $(\partial K_T/\partial P)_T$ with compression. (after Birch (**1**))

f	V/V_0	γ_G/γ_{G0}	α/α_0	$(\partial K_T/\partial P)_T$
0	1	1	1	4
0.05	0.867	0.885	0.595	3.57
0.10	0.760	0.820	0.402	3.31
0.15	0.674	0.770	0.289	3.15
0.20	0.604	0.738	0.220	3.03
0.25	0.544	0.710	0.172	2.94
0.30	0.494	0.694	0.140	2.87

Grüneisen's ratio and thermal expansion for several minerals are shown in Table 2.2.

Table 2.2 Grüneisen's ratio and thermal expansion for a few minerals (ordinary temperature and pressure).

Mineral	$\alpha\times10^6$ ($\deg^{-1}$)	γ_G
Quartz	40	0.8
Rutile	24	1.7
Corundum	18	1.7
Periclase	30	1.6
Diamond	2.9	1.0
Pyrite	27	1.6
Zircon	9	0.4
Beryl	5	0.4
Albite	17	0.5
Anorthite	15	0.7
Diopside	20	0.8
Olivine (Forsterite)	25	1.2

Since $V/V_0=0.6\sim0.7$ at the base of the earth's mantle, $\gamma_G=1.5\sim1.1$ and $\alpha=2\sim0.4\times10^{-5}\,\deg^{-1}$ in the mantle, as will be seen from Table 2.1 and Table 2.2. Then, if we assume the temperature to be several thousand degrees and its gradient to be 1°/km, the second term in (2.14) is less than unity and the third term is about 0.2~0.1. Therefore, the main feature of the variation of $1-g^{-1}d\phi/dr$ with depth should be explained by the variation of $(\partial K_T/\partial P)_T$ with depth.

$1-g^{-1}d\phi/dr$ can be estimated only from the variations of seismic velocities with depth, for g is nearly constant throughout the earth's mantle. The results of calculations are shown in Fig. 2.6. We see from this figure that $1-g^{-1}d\phi/dr$ has its maximum amounting to about 10 in the C layer and does not decrease with compression according to the fashion of $(\partial K_T/\partial P)_T$ shown in Table 2.1. Therefore, Eq. (2.14) does not hold in the C layer. And Birch has derived the conclusion that the C layer is not homogeneous. But his conclusion must be revised by the one that the C layer does not satisfy the condition of homogeneity or adiabaticity, or both.

2.2. Negative evidences against the hypothesis of inhomogeneous C layer

We have pointed out that Birch (**1**) attributed the irregularity of the C layer to the inhomogeneity from his study of the distribution of $1-g^{-1}d\phi/dr$. But the existence of the inhomogeneous C layer has been demanded from the fact that there must be the core having mass of outward concentration if we calculate the density distribution by means of Williamson-Adams' method (Chapter 2, Section 1). Bernal (**7**) and Jeffreys (**8**) have suggested that the orthorhombic olivine transforms into cubic olivine having spinel structure. But in this case, the increase of ϕ_0 shown in Fig. 2.5 must be accompanied with the increase of density. Furthermore, it is desirable

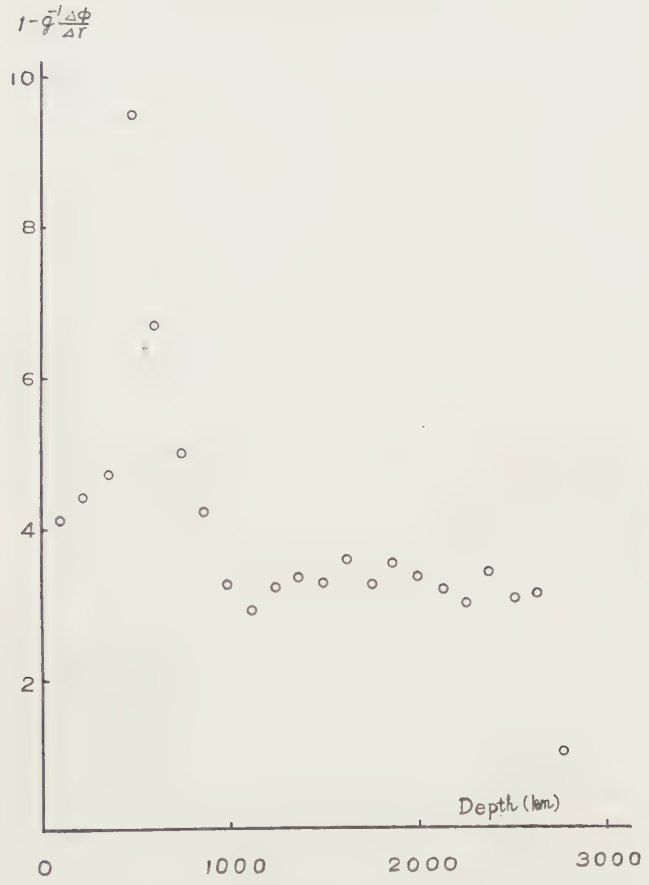

Fig. 2.6 Distribution of $1-g^{-1}d\phi/dr$.

to explain that the change occurs over the region about some hundred kilometers. With a conservative allowance for the effect of temperature, we must require for ϕ_0 about 60 $(km/sec)^2$ at room temperature, but there are only few minerals which satisfy the requirement for ϕ_0.

Table 2.3 shows that few oxides such as corundum and rutile have values of ϕ_0 of the right order. Birch (**1**) has proposed a few possibilities concerning the high-pressure phases: pyroxene, for example, enstatite, $MgSiO_3$, might adapt a structure of the corundum (Al_2O_3) type; or SiO_2 might exist at high pressure in the rutile structure. The orthosilicates such as Mg_2SiO_4 might transform into the spinel structure, or break down into high-pressure phases having the compositions MgO and $MgSiO_3$, and so on. Then he has suggested a system of several major components, for example, MgO–FeO–SiO_2. The gradual change is interpreted by him as a shift with pressure in the relative proportions of high-pressure and low-pressure phases.

Table 2.3 $(K_T/\rho)_0$ (at room temperature, one atmosphere). (after Birch (**1**))

Oxides:		Silicates:	
Periclase	47	Albite	20
Corundnm	69	Orthoclase	18
Magnetite	37	Jadeite	39
Hematite	32	Spodumene	45
Rutile	50	Anorthite	33
Quartz (α)	14	Diopside	28
		Enstatite	29
Sulfides:		Hyperstene	28
Marcasite	26	Forsterite	36
Pyrite	29	Fayalite	26
Oldhamite	16	Andradite	43
Sphalerite	19	Grossularite	45
Galena	7	Pyrope	44
		Almandite	40
		Beryl	67

But the result of the calculation of K/ρ based on the atomic theory of elasticity (Shima (**15**)) contradicts the expectation of past days. He assumed that the composing material of the B layer, having body-centred lattice structure, transforms gradually into the face-centred lattice structure in the C layer and this transition ceases at the top of the D layer. The result of calculation shows that the increase of the calculated value of K/ρ in the B layer is smaller than that of the observed one as shown in Fig. 2.7 schematically. The feature of the actual change of structure in the C layer cannot be known and the whole material composing the lower part of the B layer should not transform even though the phase transition in the C layer occurs actually, and then the above calculation for the special case cannot be applied to the actual earth. But this calculation shows that the phase transition usually considered is difficult to give rise to the necessary increase of K/ρ.

Then how should it be considered if the change of composition, i.e., the increase of the ratio of content of heavy element for the C layer is assumed? Since the breadth of the C layer amounts to about some hundred kilometers, it should be understood that the change of composition must occur gradually throughout the C layer. If we can neglect the effect of temperature, the density variation in the C layer can be obtained by means of the same procedure after Shimazu (**16**). But even if the consistent result for the density distribution of the earth's mantle can be obtained by assuming the adequate mixing ratio of heavy element with the light one, the question of the high elasticity for the D layer is remained as having no explanation. Furthermore, contrary to our expectation, there are some experimental evidences which

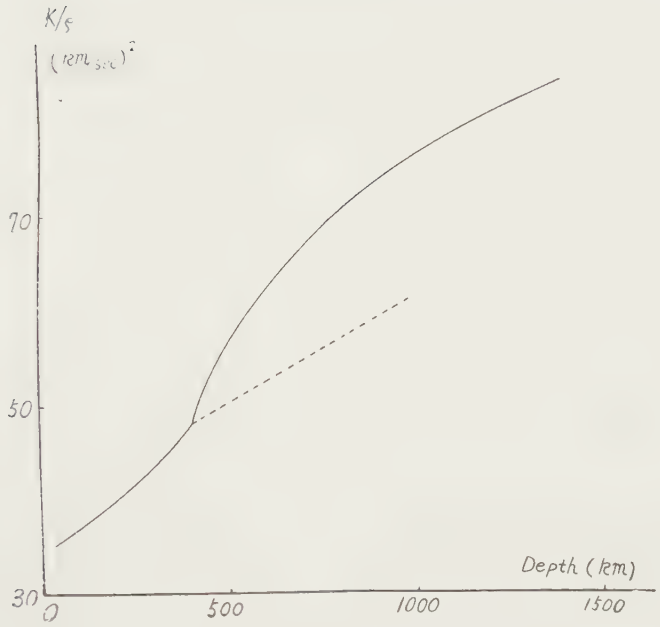

Fig. 2.7 Distribution curve of K/ρ.
—— observed, ····· calculated.

show that the increase of the content of heavy element reduces the velocity of elastic wave.

For instance, Adams (**17**) obtained the following result from the measurements of compressibilities of olivine series.

Table 2.4 Wave velocity for olivine series (km/sec)

Pressure (bars)	Forsterite (Mg_2SiO_4)	50% Fo ; 50% Fa	Fayalite (Fe_2SiO_4)
1	8.1	7.4	6.6
15000	8.6	7.9	7.1

From this table we see that the increase of heavy element (Fe) gives rise to the decrease of velocity contrary to our expectations.

On the other hand, we see the relationship between the mean atomic weight for the atoms added to $n SiO_2$ in silicates and the observed values of $(K_T/\rho)_0$ in Fig. 2.8. The values of mean atomic weight are estimated as follows:

							M	$(K_T/\rho)_0$
Albite	Na_2O	Al_2O_3	$6SiO_2$:	23.0×2	27.0×2	16.0×4 :	20.5	20
Spodumene	Li_2O	Al_2O_3	$4SiO_2$:	6.9×2	27.0×2	16.0×4 :	16.5	45
Anorthite	CaO	Al_2O_3	$2SiO_2$:	40.1	27.0×2	16.0×4 :	22.6	33
Enstatite	MgO		SiO_2 :	24.3		16.0 :	20.2	29

The increase of the mean atomic weight reduces the value of $(K_T/\rho)_0$ as we see in Fig. 2.8. However, since this rule is obtained by fixing $n\mathrm{SiO_2}$, the relation between the mean atomic weight as a whole and $(K_T/\rho)_0$ is not obvious.

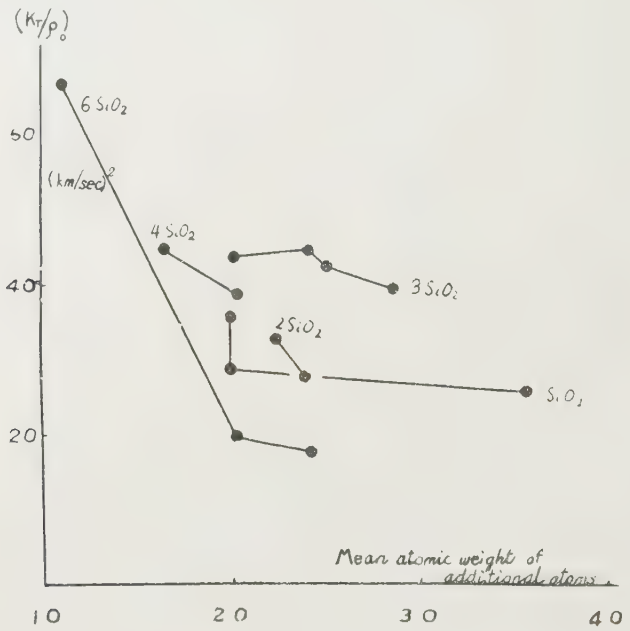

Fig. 2.8 K_T/ρ *versus* mean atomic weight of atoms added to $n\mathrm{SiO_2}$ in silicates.

2.3. Incompressibility and its pressure coefficient

We have seen that the variation of $1-g^{-1}d\phi/dr$ with depth could be traced mainly by the change of $(\partial K_T/\partial P)_T$ with depth if the earth's mantle was homogeneous and in the state of hydrostatic equilibrium. Birch's conclusion that the C layer is not homogeneous depends on the validity of the variation of $(\partial K_T/\partial P)_0$ with compression as shown in Table 2.1. The numerical values in Table 2.1 were derived from the following formula

$$\left(\frac{\partial K_T}{\partial P}\right)_T = \frac{12+49f}{3(1+7f)}, \tag{2.15}$$

which has been deduced by the theory of finite strain. This shows that $(\partial K_T/\partial P)_T$ is independent of any specific properties of the material under consideration, and all materials obeying (2.15) have an initial value $(\partial K_T/\partial P)_T=4$ which decreases monotonically.

Ramsey (**18**) considered $(\partial K_T/\partial P)_T$ from the point of view of the theory of solids. If we assume the repulsive and attractive interactions of the following types:

$$w(x)=\frac{a}{x^n}, \quad r(x)=-\frac{b}{x^m}, \quad (0<m<n) \tag{2.16}$$

where a, b are constants and x is the interatomic distance, $(\partial K_T/\partial P)_T$ has the maximum value

$$\frac{1}{3}(m+n+6), \tag{2.17}$$

and decreases monotonically with pressure to

$$\frac{1}{3}(n+3). \tag{2.18}$$

Hence, ionic crystals with m equal to unity will not show a pronounced anomaly even at low pressures, but the anomaly will be serious for metals as well as for few valence and molecular crystals with m greater than unity. On the other hand, the value of n increases fairly uniformly with the weight of the consituent atoms. For salts composed of only the lightest atoms, such as lithium fluoride, n has the value of 6 and for crystals with only heavy ions, such as cesium iodide, n is equal to 12. These considerations show that $(\partial K_T/\partial P)_T$ is not independent of the materials and the effect of compression decreases the effect of the attractive interaction. We see from (2.17) and (2.18) that the value of $(\partial K_T/\partial P)_T$ cannot be smaller than one-half of its maximum value. But the maximum value of $1-g^{-1}d\phi/dr$ is about three times the ordinary one (Fig. 2.6). Nevertheless, the qualitative result due to Birch is supported by these studies.

According to the result of calculation by use of the experimental data due to Bridgman (**19**), however, (2.15) does not hold for many silicates, i.e., $(\partial K_T/\partial P)_T$ at zero prossure is 1.7~7.5 and $(\partial K_T/\partial P)_T$ increases with increasing pressure.

Table 2.3 $(\partial K_T/\partial P)_T$ for silicates (after Verhoogen (**20**))

Silicates	K_0 (kg/cm^2)	$(\partial K_T/\partial P)_{T,0}$
Orthoclase	0.57×10^6	1.7
Labradorite	0.73	2.3
Hypersthene	0.94	7.5
Olivine	1.25	2.1
Garnet	1.37	7.1

As shown in Verhoogen's calculation, it is difficult to obtain the value of $(\partial K_T/\partial P)_T$ experimentally. Then, it seems that the conclusion on the physical constitution of the C layer obtained by the consideration of $1-g^{-1}d\phi/dr$ (Birth (**1**)) has not the experimental support.

3. Hypothesis of homogeneous earth

We have seen the opinions that the C layer is not homogeneous. The distribution of $1-g^{-1}d\phi/dr$ (Birch (**1**)), the calculations of velocities of seismic waves (Birch (**13**)) and the density distribution based on Williamson-Adams-Bullen's method (Birch (**12**)) have been thought as the evidences to show that these opinions are valid (**1, 12, 13**). These calculations are based on the assumptions that the earth's mantle satisfies the hydrostatic relation

$$dP=-g\rho dr\,. \tag{3.1}$$

The method developed in this chapter shows that the distributions of density and seismic velocities can be obtained without this assumption. Then the results obtained in this chapter show that the abnormal character of the C layer can be explained by the non-hydrostatic equilibrium state of the layer instead of its inhomogeneity.

3.1. Variation of Grüneisen's ratio with depth

We calculate the variation of Grüneisen's ratio γ_G within the earth by considering the pressure effect on it alone, since the temperature effect on Grüneisen's ratio is known to be small. The experimental estimation of the pressure effect has not yet been performed and we can rely only on the theoretical one.

We can get the relationship between γ_G and the molar volume V if the relation between Debye's maximum frequency ν_m and V or the relation between v_p, v_s and V are known, for the definition of Grüneisen's ratio is as follows:

$$\gamma_G=-\frac{\partial \log \nu_m}{\partial \log V}\,, \tag{3.2}$$

where

$$\nu_m=\left(\frac{9}{4\pi}\frac{N}{V}\frac{1}{\frac{1}{3}v_p^{-3}+\frac{2}{3}v_s^{-3}}\right)^{1/3}, \tag{3.3}$$

N being Loschmidt's number and v_p, v_s velocities of longitudinal and transversal, elastic waves, respectively.

Birch has shown (**13**) that

$$\frac{V_0}{V}=(1+2f)^{3/2}\,, \tag{3.4}$$

$$v_p^2=v_{p0}^2(1+2f)\left\{1+f\frac{11m+10}{m+2}\right\}, \tag{3.5}$$

$$v_s^2=v_{s0}^2(1+2f)\{1+f(3m+4)\}\,, \tag{3.6}$$

where f is the negative strain and $m=\frac{v_{p0}^2}{v_{s0}^2}-2$, v_0 and v_{p0}, v_{s0} being the molar volume, velocities of longitudinal and transversal waves at zero pressure, respectively.

We can obtain the following expression for γ_G by inserting the above relations into (3.2) and (3.3):

$$\gamma_G=\frac{1}{3}+\frac{1}{3}\frac{1}{v_{s0}^3\sqrt{\{1+f(3m+4)\}^3}+2v_{p0}^3\sqrt{\left\{1+f\frac{11m+10}{m+2}\right\}^3}}\left[v_{s0}^3\sqrt{\{1+f(3m+4)\}^3}\,\frac{\frac{1}{2}\frac{13m+4}{m+2}+2f\frac{11m+10}{m+2}}{1+f\frac{11m+10}{m+2}}\right.$$
$$\left.+v_{p0}^3\sqrt{\left\{1+f\frac{11m+10}{m+2}\right\}^3}\,\frac{3m+6+4f(3m+4)}{1+f(3m+4)}\right]. \tag{3.7}$$

On the other hand, Birch (**1**) has obtained the approximate expression for γ_G as follows. Using the expression of ν_m in terms of adiabatic bulk modulus K_S, density ρ and Poisson's ratio σ:

$$\nu_m=\text{const.}\left(\frac{K_S}{\rho^{\frac{1}{3}}}\right)^{1/2}F(\sigma)\,, \tag{3.8}$$

and the following formula for γ_G:

$$\gamma_G=\frac{\partial\log\nu_m}{\partial\log\rho}\,, \tag{3.9}$$

we can obtain the following equation

$$\gamma_G=-\frac{1}{6}+\frac{1}{2}\left(\frac{\partial K_T}{\partial P}\right)_T, \tag{3.10}$$

provided that the effect of $F(\sigma)$ on γ_G is negligible and the equality $\partial\log K_S/\partial\log\rho=(\partial K_T/\partial P)_T$ is assumed. Rewriting the second term on the right-hand side of (3.10) by means of the theory of finite strain, we get the expression for γ_G as a function of f as follows:

$$\gamma_G=-\frac{1}{6}+\frac{1}{2}\frac{12-49f}{3(1+7f)}\,. \tag{3.11}$$

We have obtained the above two relationships between γ_G and f, but the above two methods have advantages and drawbacks. Thus, in order to obtain γ_G by means of (3.7), we must know the velocities of elastic waves at zero pressure, but we have no method of estimating these values without knowing the material composing the earth's interior. On the other hand, γ_G can be obtained immediately as a function of f by using (3.11), but some errors are expected in the estimation, because in getting (3.11), we have made several neglects and assumptions. Both methods have also some errors due to the fact that the theory of finite strain is not so complete at present. Furthermore, elastic constants concerning the velocities of elastic waves are adiabatic ones, but in deriving (3.5) and (3.6), we have used the isothermal ones.

Fig. 3.1 shows the relationships between γ_G and f by means of (3.11) and (3.7) for various combinations of v_{p0} and v_{s0}. The combinations adopted are as follows:

(1) $v_{p0}=7.75$ km/sec, $v_{s0}=4.35$ km/sec.*
(2) $v_{p0}=7.60$ km/sec, $v_{s0}=4.30$ km/sec.**
(3) $v_{p0}=8.75$ km/sec, $v_{s0}=4.77$ km/sec.**
(4) by means of (3.11)

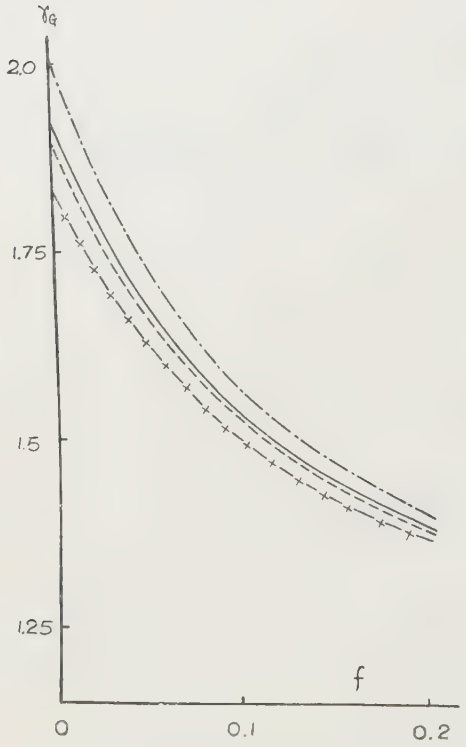

Fig. 3.1 Diagrams of Grüneisen's ratio γ_G *versus* negative strain f.
——— $v_{p0}=7.75$ km/sec, $v_{s0}=4.35$ km/sec,
····· $v_{p0}=7.60$ km/sec, $v_{s0}=4.30$ km/sec,
—·—·— $v_{p0}=8.75$ km/sec, $v_{s0}=4.77$ km/sec,
—×—×— by means of (3.11).

We see from this figure that Grüneisen's ratio derived from (3.11) and (3.7) for various combinations of v_{p0} and v_{s0} decreases with increasing negative strain in nearly the same manner.

In order to obtain the relationship between the depths and Grüneisen's ratio or negative strain, we divide the earth's mantle into many thin spherical shells. We assume $f=0.000$ at the depth of 33 km. The material at the depth of 33 km is, of course, not in the strainless state, but we have no method of determining f at this level and are obliged to take a convenient value. We put the inner boundary of the first spherical shell at the depth where $f=0.005$. We assume in this spherical shell that the composition and structure of material does not change and Grüneisen's hypothesis (Slater (**11**)):

$$\nu=\frac{\text{const}}{V^{\gamma_G}} \tag{3.12}$$

holds. Then, by inserting (3.3) into (3.12), we obtain the following equation

$$\left(\frac{V_1}{V_2}\right)^{3\gamma_G-1}=\frac{(v_p^{-3}+2v_s^{-3})_1}{(v_p^{-3}+2v_s^{-3})_2}. \tag{3.13}$$

Here, we have put Debye's maximum frequency ν_m equal to the lattice frequency ν

* Seismic velocities at depth of 33 km after Bullen (**9**).

** Seismic velocities adopted by Birch (**13**) at zero pressure for the regions shallower and deeper than the depth of 474 km respectively.

(Uffen (**21**)). Suffices 1 and 2 denote respectively the physical quantities at the inner and outer surfaces of the spherical shell. The left-hand side of (3.13) can be estimated, since the values of f at the outer and inner surfaces of the spherical shell and the mean value of γ_G are known. The denominator of the right-hand side of (3.13), $(v_p^{-3}+2v_s^{-3})_2$, is the value at the outer surface of the first shell, i.e., at the depth of 33 km, and can be estimated from the observed seismic velocities. Thus, we can estimate the value of $(v_p^{-3}+2v_s^{-3})_1$ in (3.13). We can estimate the depth of inner surface of the first spherical shell provided that we have the relationship between the depth and $(v_p^{-3}+2v_s^{-3})$ beforehand (Fig. 3.2).

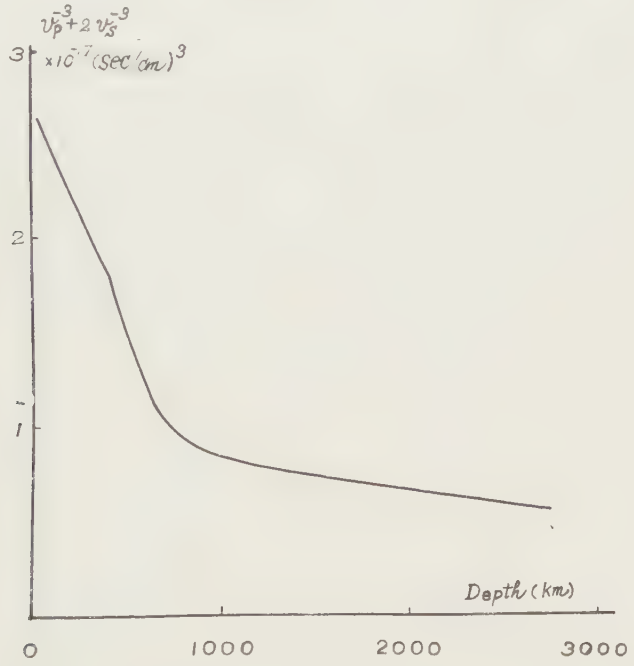

Fig. 3.2 Diagram of $v_p{}^{-3}+2v_s{}^{-3}$ *versus* depth.

The second spherical shell is formed as follows. We may consider that the strain at the outer surface of the second spherical shell is equal to the one $f=0.005$, at the inner surface of the first spherical shell, since the strain of the material is continuous within the homogeneous mantle of the earth. We put the inner surface of the second spherical shell at the depth where $f=0.015$. The value of $(v_p^{-3}+2v_s^{-3})_2$ at the outer surface of the second spherical shell is known from Fig. 3.2. The mean value of γ_G in this shell can be known from Fig. 3.1 and the value of V_1/V_2 from (3.4), for the strain in this shell is assumed to be between 0.005 and 0.015. Using the values estimated as above, we can obtain the depth which corresponds to the inner surface

of the second spherical shell in the same way as in the first spherical shell.

The boundaries of the spherical shells in the other parts of the earth's mantle can be determined in the same manner. This division of the earth's mantle depends on the assumptions that the composition, structure and Grüneisen's ratio are constant in each shell, but not necessarily the same among them, and the strains are continuous at the boundaries of the spherical shell. The accuracy of the result can be raised if we divide the earth's mantle into narrower strain ranges. Table 3.1 shows the relations among negative strain, Grüneisen's ratio and depth. The calculations are performed by use of γ_G obtained

(1) from the assumption that $v_{p_0}=7.75$ km/sec, $v_{s_0}=4.35$ km/sec

and

(2) from Eq. (3.11).

Hereafter the calculations will be done for these two cases unless otherwise noted. But the results for other cases are not so different from those in Table 3.1.

Table 3.1 Relations among the depth h, negative strain f and Grüneisen's ratio γ_G.

f	(1)		(2)	
	h (km)	γ_G	h (km)	γ_G
0	33	1.92	33	1.83
	102		98	
0.01		1.85		1.78
	235		226	
0.02		1.80		1.73
	355		340	
0.03		1.75		1.69
	443		432	
0.04		1.70		1.65
	502		489	
0.05		1.67		1.62
	552		539	
0.06		1.63		1.59
	595		582	
0.07		1.60		1.56
	678		647	
0.08		1.57		1.53
	758		726	
0.09		1.55		1.51
	872		797	
0.10		1.52		1.49
	1050		952	
0.11		1.50		1.47
	1330		1171	
0.12		1.48		1.45
	1656		1460	
0.13		1.46		1.44
	2013		1789	
0.14		1.45		1.42
	2389		2145	
0.15		1.43		1.41
	2790		2505	
0.16		1.42		1.39

The values near the earth's surface are rather large, compared with the ones of Grüneisen's ratio of some minerals shown in Table 2.2. The reason for this discrepancy is not known.

3.2. Variations of seismic velocities and density with depth

The distributions of the seismic wave velocities can be obtained by means of (3.5), (3.6) and Table 3.1 (Fig. 3.3). The solid lines in Fig. 3.3 show the observed values. We see that the black points calculated by the present method is fairly good approximation to the variations of seismic velocities with depth. Therefore, the variation of seismic velocities in the earth's mantle can be explained by the hypothesis of homogeneous earth. As we have seen in Chapter 2, Section 1, Birch (**13**) has obtained the relation between depth and negative strain, and calculated the distributions of seismic velocities, assuming that the earth's mantle is isothermal, homogeneous and in the state of hydrostatic equilibrium. But he adopted the different initial velocities corresponding to the B and D layers, because the steep increase of seismic

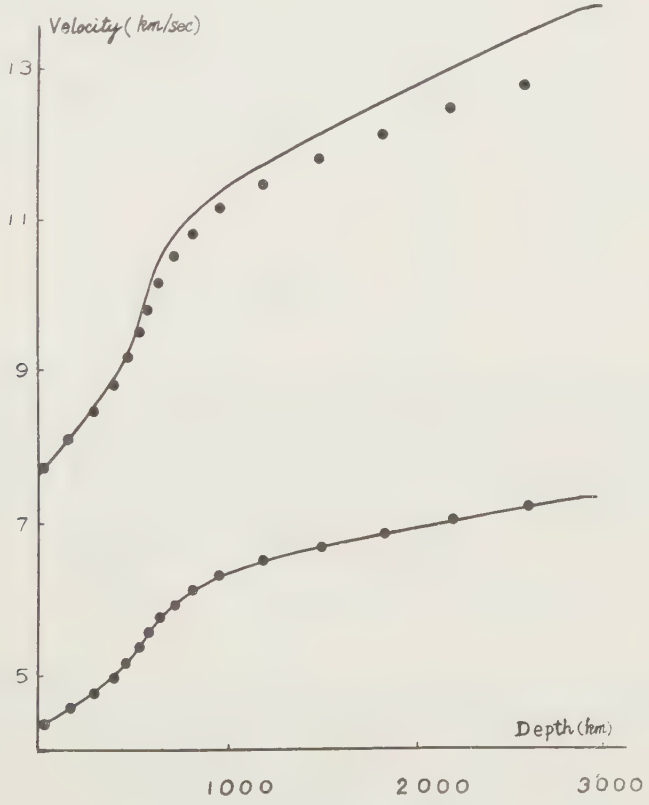

Fig. 3.3 Distribution of seismic velocities. Solid lines show the observed values.

velocities in the C layer could not be explained by the above assumptions. Fig. 3.3 shows that the assumption of homogeneous mantle can explain the distributions of seismic velocities and the steep increase of seismic velocities in the C layer.

Figs. 2.3 and 3.3 were drawn by use of (3.5) and (3.6) which involve no temperature effect. Nevertheless, the fact that rather satisfactory results have been obtained means that the temperature do not seriously affect the distributions of seismic velocities in the earth's mantle. This fact suggests also the difficulties to estimate the exact value of temperature within the earth by means of the distributions of seismic velocities alone. The same can be said on the inhomogeneity of the material composing the earth's mantle. Shimazu (**22**) suggests that the effect of the third order term of finite strain may explain the discrepancies between the calculated and observed values. But the effects of temperature, composition and phase change are also available and it is difficult to determine the factor which most prominently affects the velocities. At present, however, there is no study of this sort and it is the tendency to estimate the orders of these secondary effects, assuming no other effects but one, from the difference between observed and calculated values (**16**, **22**).

The ratio of density at the outer surface to that at the inner surface of each spherical shell can be obtained from Table 3.1 and Eq. (3.4) (Table 3.2).

The density distribution, mass and moment of inertia of the earth's mantle can be estimated, taking the density ρ_{33} at the depth of 33 km as a parameter. The results of calculations are

$$(1)\quad M_m = 1.147\ \rho_{33}\times 10^{27}\ \text{gr}, \qquad I_m = 2.024\ \rho_{33}\times 10^{44}\ \text{gr. cm}^2,$$
$$(2)\quad M_m = 1.159\ \rho_{33}\times 10^{27}\ \text{gr}, \qquad I_m = 2.047\ \rho_{33}\times 10^{44}\ \text{gr. cm}^2.$$

The mass and the moment of inertia of the earth's core can be obtained, taking the central density ρ_c as a parameter provided that the density distribution in the earth's core can be obtained by Williamson and Adams' method. Thus, the mass and the moment of inertia of the earth can be expressed by using two parameters ρ_{33}, ρ_c. These parameters can be settled by the observed values for the mass and the moment of inertia of the earth. The results of the calculation are as follows:

$$(1)\quad \rho_{33} = 3.46\ \text{gr/cm}^3, \qquad \rho_c = 12.41\ \text{gr/cm}^3,$$
$$(2)\quad \rho_{33} = 3.42\ \text{gr/cm}^3, \qquad \rho_c = 12.44\ \text{gr/cm}^3.$$

By using the above values and the results in Table 3.2, we get the density distribution within the earth as shown in Table 3.3. The distribution of acceleration of gravity can be calculated by means of the density distribution and (1.3).

The above results of calculations show that the observed value of mass and moment of inertia of the earth can be interpreted satisfactorily by the hypothesis of

Table 3.2 The ratio of density at the outer suriface to that at the inner surface of each spherical shell.

Shell number	ρ_2/ρ_1	Depth (km)	
		(1)	(2)
		33	33
1	0.9852	102	98
2	0.9710	235	226
3	0.9716	355	340
4	0.9721	443	432
5	0.9726	502	489
6	0.9731	552	539
7	0.9736	595	582
8	0.9740	678	647
9	0.9745	758	726
10	0.9749	872	797
11	0.9753	1050	952
12	0.9757	1330	1171
13	0.9761	1656	1460
14	0.9765	2013	1789
15	0.9769	2389	2145
16	0.9772	2790	2505
17	0.9775		

homogeneous earth even if we do not assume the abnormally high value of density at the depth of 33 km, or the discontinuous or steep increase of density in the C layer. Therefore, it is not reasonable to conclude that the earth's mantle should involve the inhomogeneous region (**1**, **12**, **13**) by the consideration of initial density derived from the assumption of hydrostatic relation and adiabatic temperature gradient.

3.3. Temperature distribution within the earth's mantle

But the hypothesis of homogeneous mantle of the earth denies the hydrostatic relation as follows.

If we assume that the temperature increases with increasing depth, we find, from the equation:

$$\frac{dP}{dr}=\left(\frac{\partial P}{\partial V}\right)_T\frac{dV}{dr}+\left(\frac{\partial P}{\partial T}\right)_V\frac{dT}{dr}, \tag{3.14}$$

Table 3.3 Distributions of density and acceleration of gravity within the earth.

(1)			(2)		
Depth (km)	Density (gr/cm^3)	Acceleration of gravity (cm/sec^2)	Depth (km)	Density (gr/cm^3)	Acceleration of gravity (cm/sec^2)
33	3.46	979	33	3.42	979
102	3.52	982	98	3.47	982
235	3.62	984	226	3.58	984
355	3.73	985	340	3.68	986
443	3.83	986	432	3.79	987
502	3.94	986	489	3.90	988
552	4.05	986	539	4.00	988
595	4.16	986	582	4.11	988
678	4.27	985	674	4.22	987
758	4.38	983	726	4.33	986
872	4.50	981	797	4.44	984
1050	4.61	977	952	4.56	981
1330	4.73	974	1171	4.67	970
1656	4.84	977	1460	4.79	976
2013	4.96	990	1789	4.90	982
2389	5.08	1022	2145	5.02	999
2790	5.19		2505	5.13	
2898			2898		
2898	9.91	1064		9.93	1066
3000	10.07	1041		10.09	1044
3200	10.37	995		10.39	997
3400	10.65	945		10.67	947
3600	10.90	892		10.92	894
3800	11.12	837		11.15	839
4000	11.33	780		11.35	782
4200	11.51	721		11.54	722
4400	11.68	660		11.71	661
4600	11.83	597		11.86	598
4800	11.96	533		11.99	534
4982	12.06	473		12.09	474
5121	12.13	427		12.16	428
5700	12.32	231		12.34	231
6371	12.41	0		12.44	0

an inequality such that

$$\frac{dP}{dr} < -\left(\frac{\partial P}{\partial V}\right)_T \frac{dV}{dr}. \tag{3.15}$$

If the condition of hydrostatic equilibrium is satisfied in the earth, the left-hand side of the inequality (3.15) should be equal to $-g\rho$. Since

$$-\left(\frac{\partial P}{\partial V}\right)_T = \frac{K_T}{V}, \tag{3.16}$$

we can obtain the value of the right-hand side of (3.15) as $K_T d(\log V)/dr$. Fig. 3.4 shows the calculated value of $K_S d(\log V)/dr$ and $g\rho$ estimated from the observed value of ϕ, density distribution (Table 3.3) and the distribution of the acceleration of gravity (Table 3.3). Fig. 3.4 shows that the inequality (3.15) is satisfied in the

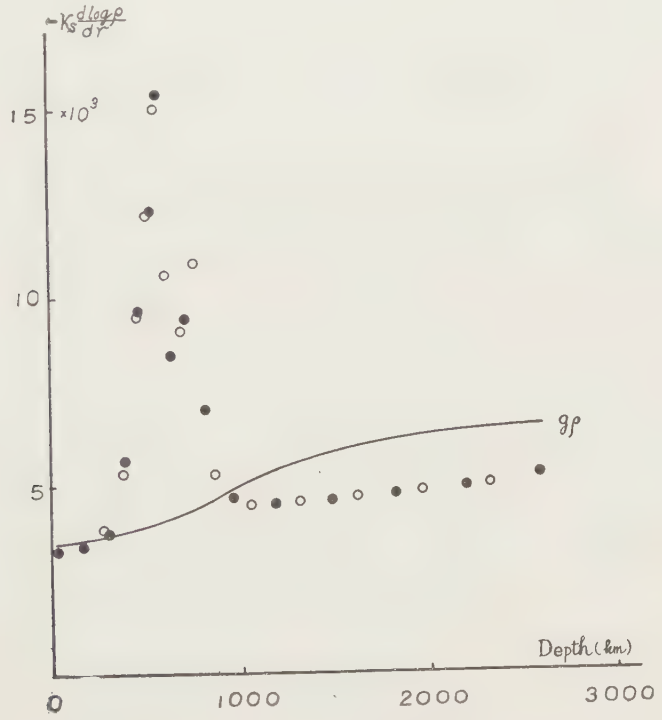

Fig. 3.4 Distributions of $K_S d(\log V)/dr$ and $g\rho$.

B and D layers, but not in the C layer. The difference of the both sides of this inequality is very large in the C layer. If we attribute this difference to the identification of K_T and K_S used in the calculation, we must conclude the abnormally large value of $T\alpha\gamma_G$ in the C layer from the following relation:

$$\frac{K_S}{K_T} = 1 + T\alpha\gamma_G. \tag{3.17}$$

The value of $T\alpha\gamma_G$ is about 0.06 if we assume $T=2000°K$, $\alpha=2\times10^{-5}\,\mathrm{deg}^{-1}$ and $\gamma_G=1.5$. Therefore, we cannot attribute this difference in the C layer between both sides of the inequality to the identification of K_T with K_S, and we must attribute this difference to the assumption that the earth's mantle is in the state of hydrostatic equilibrium.

We can estimate the distribution of temperature in the region which satisfies the inequality (3.15) (**23**). If we assume that the condition of hydrostatic equilibrium is satisfied in this region, the equation for the density change may be written as follows:

$$\frac{d\rho}{dr}=-\frac{g\rho}{\phi}+\alpha\rho\tau\,, \tag{3.18}$$

which can be approximated by

$$\frac{\rho_1-\rho_2}{r_1-r_2}=-\frac{g}{\phi}\,\frac{\rho_1+\rho_2}{2}+\alpha\tau\,\frac{\rho_1+\rho_2}{2}\,, \tag{3.19}$$

or

$$\frac{1}{r_1-r_2}\left(1-\frac{\rho_2}{\rho_1}\right)=\frac{1}{2}\left(1+\frac{\rho_2}{\rho_1}\right)\left(\alpha\tau-\frac{g}{\phi}\right). \tag{3.20}$$

Therefore, we get

$$\alpha\tau=\frac{\dfrac{1}{r_1-r_2}\left(1-\dfrac{\rho_2}{\rho_1}\right)}{\dfrac{1}{2}\left(1+\dfrac{\rho_2}{\rho_1}\right)}+\frac{g}{\phi}\,. \tag{3.21}$$

Thus $\alpha\tau$ can be estimated from this equation (3.21), since ϕ is a known quantity and g and ρ_2/ρ_1 have been estimated in Table 3.3 and Table 3.2, respectively.

On the other hand, by virtue of the following relations

$$\frac{\alpha}{C_p}=\frac{\alpha}{C_v(1+T\alpha\gamma_G)}\,, \tag{3.22}$$

and

$$\gamma_G=\frac{K_S\alpha A}{\rho C_p}\,, \tag{3.23}$$

the temperature can be expressed as follows:

$$T=\frac{1}{\gamma_G}\left(\frac{K_S}{\rho}\,\frac{A}{\gamma_G C_v}-\frac{1}{\alpha}\right). \tag{3.24}$$

We have known the value of $d\tau$ at each depth, that is, we have known α's as a function of τ at various depths. From this functional relation and Eq. (3.24), the corresponding values of T and τ can be known. In other words, we can know

τ as a function of T. Thus we can find the distribution of temperature in the earth by numerical integration of Eq. (1.5) after substituting the above functional relation between T and τ. The results of calculations are given in Table 3.4.

Table 3.4 Absolute temperature within the earth.

Depth (km)	(1)		(2)	
1000	2000*	3000*	2000*	3000*
1200	2312	3340	2292	3321
1400	2696	3749	2651	3705
1600	3110	4186	3048	4125
1800	3558	4655	3484	4582
2000	3989	5107	3899	5019
2200	4478	5616	4373	5512
2400	4899	6058	4782	5942
2600	5384	6563	5251	6431
2800	5922	7120		

In the calculations, the value of 20 is assumed for the mean atomic weight of the composing material of the D layer and C_v at high temperature, such as in the earth's interior, is 2.49×10^8 erg. deg^{-1} mol^{-1} by Dulong-Petit's law.

3.4. Deep focus earthquakes

We have seen that the hypothesis that the earth's mantle is homogeneous and not in the state of hydrostatic equilibrium can explain reasonably the observed facts. Furthermore, this hypothesis is important in relation to the existence of the deep focus earthquakes in the C layer. In this case, the magnitude and the direction of the force added to the gradient of pressure should be noted. This force acts towards the direction to which the apparent acceleration of gravity increases and its maximum magnitude amounts to about twice the acceleration of gravity (see Fig. 3.3). Therefore, it seems that the region deeper than the depth of 1000 km is strangled by the spherical shell of about some hundred kilometers breadth beginning from the depth of about 400 km. In that spherical shell, the force is the greatest at the middle and decreases towards both boundaries.

But this hypothesis proposed in order to explain the abnormal character of the C layer must be examined for a while. Formerly we have connected the existence of deep focus earthquake in the C layer with the non-hydrostatic equilibrium, but it is uncertain that the abnormality of the C layer which spreads over the world directly concerns with the number or the energy of the deep focus earthquakes

* These are assumed values.

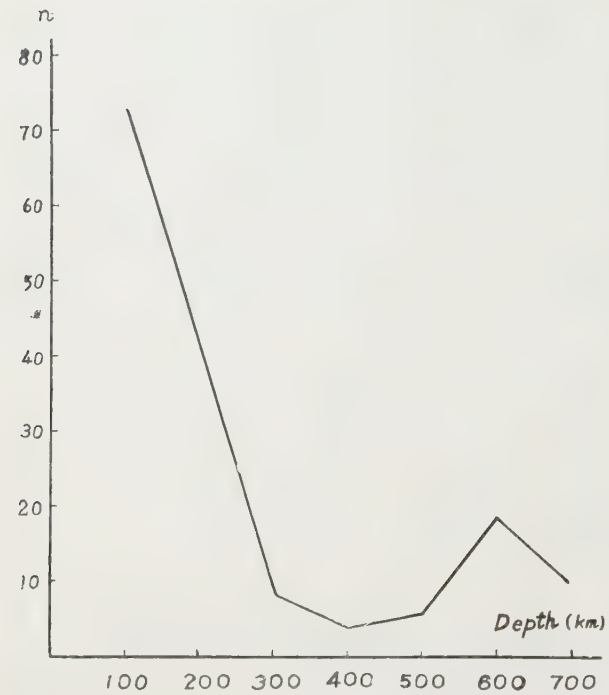

Fig. 3.5 Total number of the more important earthquakes at different levels in the earth's mantle beneath the Indonesian Archipelago for the period 1904～1945. (after Ritsema (**24**))

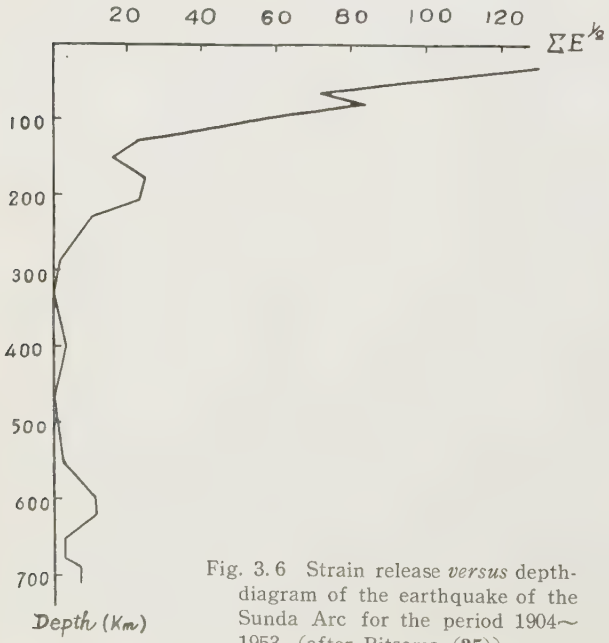

Fig. 3.6 Strain release *versus* depth-diagram of the earthquake of the Sunda Arc for the period 1904～1953. (after Ritsema (**25**))

located at the special place and depth. Nevertheless, it is interesting to see whether this abnormal properties of the C layer promote the occurrence of deep focus earthquakes. According to the statistical studies by Ritsema (**24**, **25**), the number and the strain release of deep focus earthquakes have the singular distribution in the C layer, compared with others. But it is the task for the future to study whether or how the condition of non-hydrostatic equilibrium concerns with these phenomena.

We have the negative evidences to the hypothesis that the composition or structure changes gradually in the C layer. But we are anxious about the following questions: "Why only the C layer is in the state of non-hydrostatic equilibrium and in what state is the B layer which is shallower than the C layer?" We shall have an apportunity to consider the B layer.

4. Various problems and questions

The difference between the two calculated values in Fig. 3.4 $\left(g\rho, K_S \frac{d \log V}{dr}\right)$ is due to the effect of temperature. Of course, this can be interpreted as the effects of composition or phase change, but the relation between the elastic constants and these effects is not obvious, and the experimental and theoretical studies of this relation are in the negative direction to the result of seismic evidences (see § 2.2). Therefore, we do not consider these effects. Since, at high temperature,

$$\left.\begin{aligned} \left(\frac{\partial P}{\partial T}\right)_V &= \frac{C_v \gamma_G}{V}, \\ C_v &= 2.49 \times 10^8 \text{ erg. deg}^{-1} \text{ mol}^{-1}, \end{aligned}\right\} \tag{4.1}$$

the temperature gradient can be obtained by Eq. (3.15), Fig. 3.4 and Table 3.3 (Fig. 4.1). The C layer is excluded from the numerical calculations, because the hydrostatic relation $dP = g\rho dr$ is not satisfied in this layer. Though Fig. 4.1 is the result of rough calculation taking $K_S = K_T$, the method of exact calculation should be referred to § 3.3. We see in Fig. 4.1 that the temperature gradient in the D layer is about

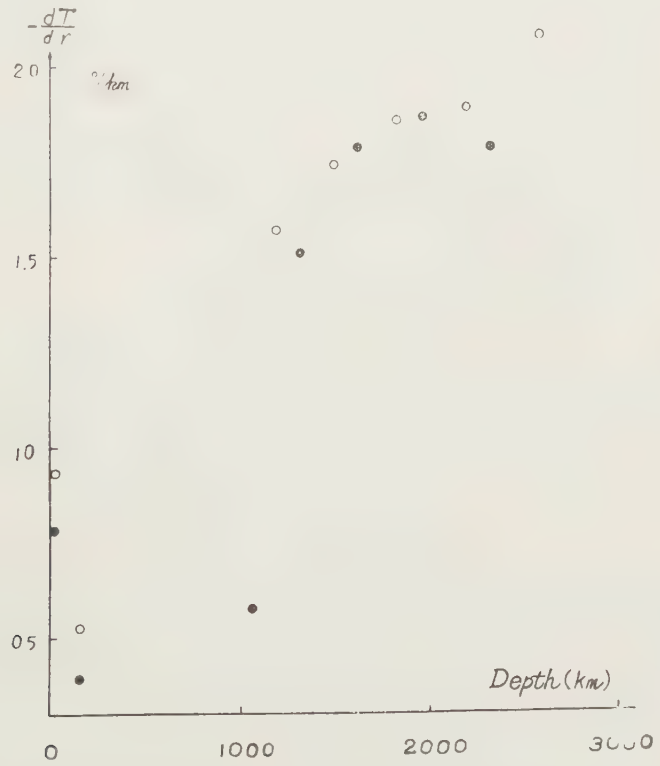

Fig. 4.1 Distribution of temperature gradient.

1.8°/km and that the one in the B layer is about 0.9°/km at the top and decreases to zero with increasing depth. Since the temperature gradient in the B layer must be greater than that in the D layer from Jeffreys' proposal on the thermal origin of the earth which advocates the crustal concentration of radioactive contents, the above result conflicts with Jeffreys' proposal.

But this result may depend on the velocity distribution. At present, the disagreement on the velocity distribution in the B layer exists among seismologists, so that it is not good to derive the impetuous conclusion. Therefore, let us examine the properties of the B layer by use of the various velocity distributions (**3**, **4**, **27**), for instance, the following distributions (Table 4.1).

Table 4.1 Velocities of P and S waves in the upper mantle. (km/sec)

Depth	V_p				V_s			
(km)	H	N	G	J	H	N	G	J
50	7.59'	8.0	8.0	7.8	4.44	4.45	4.46	4.36
100	7.93	7.85	7.9	7.95	4.56	4.4	4.44	4.45
150	8.02	7.9	7.9	8.1	4.61	4.35	4.46	4.5
200	8.14	8.1	8.1	8.3	4.65	4.4	4.5	4.6
250	8.28	8.3	8.4	8.45	4.73	4.45	4.6	4.7
300	8.48	8.5	8.6	8.6	4.82	4.6	4.7	4.75
400	8.97	9.0	9.1	9.0	5.10	4.95	4.95	4.9
500	9.63	9.6	9.6	9.7	5.44	5.3	5.3	5.3

H: after Honda, Sagisaka and Takehana,
N: after Gutenberg (1953, (**4**)),
G: after Gutenberg (1948),
J: interpolated values from Jeffreys' solution (**3**).

These solutions resemble to each other except H, but the decrease of velocity at the neighbourhood of the depth of 100 km is found in N and G but not in H and J. This fact gives rise to the great difference about the interpretation on the physical properties of the upper mantle derived from the seismic velocities.

The numerical value of V_1/V_2 in the upper mantle can be obtained by means of (3.13) and Grüneisen's ratio assumed, for instance, to be 1.5. In this case, it is convenient in the numerical calculation to take the boundaries of the spherical shells at the depths as shown in Table 4.1. We must take suitable value of Grüneisen's ratio unavoidably, but this does not affect seriously the qualitative result as far as we do not take abnormal value of Grüneisen's ratio.

If the condition of hydrostatic equilibrium is satisfied and if the material composing the upper mantle is homogeneous, we should obtain by (3.14) and (3.16)

$$g > \frac{K_T}{\rho}\frac{d\log V}{dr}. \tag{4.2}$$

If we use the approximation $K_T/\rho \approx \phi = K_S/\rho$, the right-hand side of Eq. (4.2) can be calculated from seismic velocities and (3.13). Fig. 4.2 shows the results obtained by use of the four sorts of velocity distributions tabulated in Table 4.1.

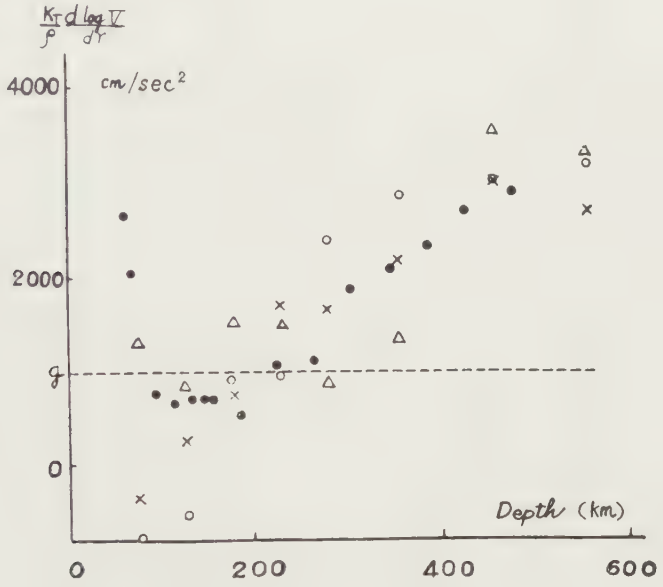

Fig. 4.2 Distributions of g and $\phi d(\log V)/dr$ for various distributions of seismic velocities.
● Honda et al.,
× Gutenberg (1948),
△ Jeffreys,
○ Gutenberg (1953).

It will be seen that the proposal that the following region can be understood as homogeneous and in the state of hydrostatic equilibrium:

H: 90 km~200 km
N: 50 km~250 km
G: 50 km~200 km

does not conflict with the result of calculation. But the region shallower than the depth of 90 km and deeper than the depth of 200 km in case H, deeper than the depth of 250 km in case N, deeper than 200 km in case G and the whole upper mantle in case J cannot be interpreted as homogeneous and in the state of hydrostatic equilibrium. In three cases which can be interpreted as homogeneous and in the state of hydrostatic equilibrium, the temperature gradient can be estimated (Table 4.2).

Table 4.2 Temperature gradient in the upper mantle. (°/km)

Depth (km)	H	Depth (km)	N	G
90	1.50	75	9.48	7.21
110	1.86	125	8.25	4.02
130	1.68	175	0.58	1.43
150	1.68			
180	2.45			

According to Jeffrey's proposal on the thermal origin of the earth, the temperature gradient in the upper mantle should be great on account of the crustal concentration of the radioactive contents. H having lower temperature gradient than D conflicts with this proposal and the upper mantle cannot be considered as homogeneous and in the state of hydrostatic equilibrium in case of H. Therefore, if the hydrostatic equilibrium and homogeneity condition are satisfied in the upper part of the B layer, only the two solutions due to Gutenberg can satisfy Jeffrey's proposal.

4.2. Temperature at the top and at the base of the earth's mantle

The most reasonable value of the melting point of the material composing the earth's mantle is, at present, the one derived from Uffen's method (**21**) which uses the seismic velocities.

Lindemann (**28**) proposed the following relationship between the melting point and the frequency of crystal lattice:

$$\nu = \text{const}\sqrt{\frac{T_m}{AV^{2/3}}}, \tag{4.3}$$

where A is the mean atomic weight and T_m the melting point. The numerical value of constant is found experimentally to be about 2.8×10^{12}. If we identify ν with ν_m in (3.3) and assume the mean atomic weight to be 20, the melting point at the base, depth of 2800 km, of the earth's mantle can be estimated to be 4650°K. In general, if the melting point T_m is known at the definite level, the melting point at another level can be estimated by means of the following equation

$$\frac{T_m}{T_{m0}} = \frac{A}{A_0}\left\{\frac{(v_p^{-3}+2v_s^{-3})_0}{(v_p^{-3}+2v_s^{-3})}\right\}^{2/3}, \tag{4.4}$$

which has been derived from (3.3) and (4.3). Suffix 0 indicates the quantity at the standard level. The values calculated by (4.3) and (4.4) cannot be taken as the well-established ones on account of the validity of Lindemann's formula, the identification of ν and ν_m, and the homogeneity assumption, but these values can be taken as the one obtained by means of the most reasonable method at present. The temperature within the earth's mantle should be lower than these values.

The determination of temperature at the top of mantle is at first sight a rather simple one, but the exact determination is difficult. We fortunately have some evidences which bear on the matter, such as heat flow in continental areas, which is known at least in its order of magnitude. This, together with an estimate of the radioactive content of continental rocks, makes it possible to calculate the temperature at the top of mantle. It is readily found to lie between 300° and 1000°, roughly, depending on the exact thickness of the crust and how much of the total heat flow is assumed to be generated in it. The crust of 50 km thickness with an average radioactive content about 50% larger than ordinary basalt would generate about 90% of the total heat flow, and the steady state temperature at that level would be about 775°C (**29**).

On the other hand, the average v_S for four specimens of dunite at 4000 kg/cm^2 and 30°C is 4.57 km/sec. The average pressure coefficient of this velocity, at 4000 kg/cm^2, between 30°C~100°C is about 140×10^{-6}. If we extrapolate these values linearly to 700°C and 10000 kg/cm^2 (pressure at the depth of 33 km), we find $v_S=$ 4.21 km/sec which should be compared with the "observed" value, 4.36 km/sec. Since the probable defects in this extrapolation seem likely to lead to a value which is too high rather than too low, we must take the temperature about 500°C in order to coincide with the observed value. On the other hand, we may derive a value for K/ρ at 10000 kg/cm^2 and ordinary temperature for the same dunite; that is 39.2×10^{10}, which should be compared with Jeffreys' value, 34.3×10^{10}. The difference of about 12.5 per cent may be ascribed to the effect of temperature. If this is again taken as 700°C at this level, the required temperature coefficient of K/ρ is -180×10^{-6}, which is about the value of iron and seems rather low for dunite. Again a temperature lower than 700°C is indicated if we insist upon this material and these data (**13**). But there is a limit when we discuss the difference between the observed velocity and the extrapolated one from the experimental values for rocks, because there are disagreements among seismologists on the velocities of seismic waves as we see in Table 4. 1.

The method which depends on the measurement of radioactivity of rocks or on the seismic velocities and the measurement of elastic properties of rocks cannot assure the correct answer, but it seems to give rise to only a few error even if we take 800°K~1000°K as the temperature at the top of the mantle.

Then, it is difficult to reconcile the following results

1) maximum temperature within the earth's mantle (melting point),
2) temperature at the top of the mantle,
3) temperature gradient in the D layer,
4) Jeffreys' proposal which requires the steep increase of temperature at the upper mantle.

If we insist upon these results, we must conclude that the C layer and the lower part of the B layer are nearly isothermal. But we have no evidence which prove it to be valid.

4.3. Further discussion on the temperature distribution

The pessimistic conclusion described above on the temperature distribution within the earth gives us such impression that it is difficult to derive the temperature distribution from seismic data alone. The difficulty is based on the uncertainties of seismic data and is doubled by the uncertainties of the theory of solids. The straightforward examples which show the difficulties for estimating the phenomena concerning the temperature within the earth from seismic data alone are found in Fig. 2.3 and Fig. 3.3 which were derived under the isothermal assumption. In short, it can be said that all the method of evaluation of temperature from seismic data alone treat the difference between the calculated and observed values in these figures. But this difference involves the effects due to the approximation of finite strain theory, chemical physics, the change of chemical composition and structure of material. At present, however, it is difficult to distinguish the effect between these and that of the temperature. It seems to the author that these difficulties cannot be removed until the quantitative relationships among seismic velocities, chemical composition and structure of material are established.

How can this blind alley be attacked in the theory of the internal constitutions of the earth? But we are never disappointed and the remarkable development in the theory of the internal constitution of the earth in the latest ten years encourages us. Until about fifteen years ago, the isolated theory by atomic theory after Haalck (**30**) and the germ of the method based on the theory of finite strain which was developed by Birch and Shimazu to the splendid form had been thrown lights into the studies based on the classical theory after Jeffreys and Bullen. At present, however, the methods based on the theory of finite strain and chemical physics have been developed and they are grown to the indispensable methods. On the other hand, the results in the field of astrophysics and geomagnetism have been taken in and the studies on the physical properties and state of the earth's core have greatly progressed. The contributions from seismology have been the proposals of the existence of inner core and Gutenberg's low velocity layer. These facts teach us that the progress in the theory of the internal constitution of the earth can be obtained by the continual concern to the progress in physics on which it built and the result of astrophysics, geology and geomagnetism, and the establishment of seismic evidences which treat directly the interior of the earth, and not by the craft work.

For instance, Rikitake (**31**) has proposed the method of estimating the tempera-

ture distribution by some data other than seismic velocities. He used the value of electrical conductivity in the upper mantle derived from the analysis of the variations of geomagnetic field. He used the pressure distribution due to Bullen in his calculation of temperature on the base of the assumption of homogeneity and hydrostatic equilibrium. Therefore, his process of calculation is inconsistent with the theoretical frame, but the result showing the discrepancy from adiabatic temparature gradient (assumption of Bullen's method) demands our considerations. To what should be attributed this discrepancy? (1) Is there any miss in obtaining the electrical conductivity? Can we solve this reasonably by comparing with the seismic data? (2) Does it depend on the assumption introduced in the calculation based on the theory of ionic crystal? For instance, the evaluation of activation energy, the effect of pressure on the electrical conductivity and so on? (3) The discovery of method in order to estimate the temperature from the more established data, though it is only an artificial subject. These studies will open the gate to the possibility of the evaluation of temperature distribution by use of electical conductivity which suffers the effect of temperature seriously.

5. Summary

The theory of the internal constitution of the earth has greatly progressed by the work of Willeamson and Adams who found the method of estimating the density change within the earth. This method which uses the values of seismic velocities suggests that the earh's mantle should involve the inhomogeneous region, provided we avoid the abnormal high value of density at the surface. This region has been ascribed to the C layer on account of the steep increases of seismic velocities in this layer. This conclusion is supported by the calculations of the variations of seismic velocities in the isothermal homogeneous layer, i.e., the finite strain theory can explain the variations of seismic velocities in the B and D layers, except the C layer. But these interpretations fail to explain the high value of K/ρ in the D layer, because the experimental study shows that the increase of heavy element in Olivine gives rise to the decrease of velocity of elastic wave and the theoretical study shows that the change of lattice structure into closer packed one cannot give rise to the steep increase of K/ρ in the C layer.

(1) The theory developed in this paper concludes that the earth's mantle is homogeneous and the C layer does not satisfy the hydrostatic relation. The internal force in the C layer acts towards the earth's centre and has about the magnitude twice as large as that due to gravity, i.e., the earth beneath the D layer is strangled by the layer which has the breadth of some hundred kilometers. It is interest to consider this force with respect to the existence of deep focus earthquakes in the C layer.

(2) This theory based on chemical physics can calculate the distributions of density and the velocities of seismic waves which coincide with the observed ones fairly satisfactorily. It ascribed the proposal of inhomogeneous C layer to the assumptions of Williamson and Adams' method.

(3) The characteristic feature of this theory is that it has the possibility of estimating the temperature distribution within the earth, which is assumed by the method of Williamson and Adams to be adiabatic. In general, however, the exact determination of the temperature distribution by use of the seismic velocities alone is difficult, because the temperature variation within the earth is less effective to the change of seismic velocities, and the equation of state of the material composing the earth's interior depends on the composition and lattice structure in addition to the temperature and pressure.

(4) The method of Williamson and Adams cannot be applied to obtaining the density change in the B and C layers, because the upper part of the B layer is not homogeneous and in the state of hydrostatic equilibrium, or has the high temperature gradient, and the C layer and the lower part of the B layer are not in the state of hydrostatic equilibrium.

Acknowledgement

The writer wishes to express his thanks to Professor S. Miyamoto (Astrophysics, Kyoto University) who teached him in the days when he graduated the Kyoto University about ten years ago and Professor E. Nishimura (Geophysics, Kyoto University) who gave him valuable suggestions through active discussions. His hearty thanks are also due to Professor K. Sassa (Geophysics, Kyoto University) who encouraged him throughout this work. Further, the writer wishes to express his thanks to Dr. Y. Shimazu (Earth Science, Nagoya University) and Dr. M. Shima (Abuyama Seismological Observatory, Kyoto University) who gave him valuable comments. Lastly, the writer's thanks are due to Dr. F. Birch (Dumber Laboratory, Harvard University) who gave him valuable informations through several private communications.

REFERENCES

1. F. Birch, J. Geophys. Res., **57** (1952) 227.
2. B. Gutenberg (editor), *Internal Constitution of the Earth*, New York, McGraw-Hill Book Co., Second edition, 1951.
3. H. Jeffreys, M. N. R. A. S., Geophys. Suppl., **4** (1939) 498; *ibid*, **4** (1939) 594.
4. B. Gutenberg, Bull. Seis. Soc. Amer., **43** (1953) 223; Trans. Amer. Geophys. Union, **32** (1951) 373.
5. L. H. Adams and E. D. Williamson, J. Wash. Acad. Sci., **13** (1923) 413.

6. K. E. Bullen, M. N. R. A. S., Geophys. Suppl., **3** (1936) 395; Trans. R. Soc. New Zealand, **67** (1937) 122; *ibid*, **70** (1940) 137; *ibid*, **71** (1941) 164; Bull. Seis. Soc. Amer., **30** (1940) 235; *ibid*, **32** (1942) 19.
7. J. D. Bernal, Observatory, **59** (1936) 268.
8. H. Jeffreys, M. N. R. A. S., Geophys. Suppl., **4** (1937) 50.
9. K. E. Bullen, *An Introduction to the Theory of Seismology*, Cambridge Univ. Press., 1947.
10. J. Verhoogen, Trans. Amer. Geophys. Union, **32** (1951) 41.
11. J. C. Slater, *Introduction to Chemical Physics*, New York, McGraw-Hill Book Co., 1939.
12. F. Birch, Trans. Amer. Geoppys. Union, **35** (1954) 79.
13. F. Birch, Bull. Seis. Soc. Amer., **29** (1939) 463.
14. K. E. Bullen, M. N. R. A. S., Geophys. Suppl., **5** (1949) 355.
15. M. Shima, Zisin, **8** (1955) 38 (in Japanese).
16. Y. Shimazu, J. Phys. Earth, **1** (1952) 11.
17. L. H. Adams, Beitr. Geophys., **31** (1931) 315.
18. W. H. Ramsey, M. N. R. A. S., Geophys. Suppl., **6** (1950) 42.
19. P. W. Bridgman, Proc. Amer. Acad. Arts Sci., **76** (1948) 55, 71.
20. J. Verhoogen, J. Geophys. Res., **58** (1953) 337.
21. R. J. Uffen, Trans. Amer. Geophys. Union, **33** (1952) 893.
22. Y. Shimazu, J. Earth Sci., Nagoya Univ., **2** (1954) 15.
23. H. Miki, J. Phys. Earth, **2** (1954) 1.
24. A. R. Ritsema, Indonesian J. Nat. Sci., 1953, 34.
25. A. R. Ritsema, Indonesian J. Nat. Sci., 1954, 41.
26. A. R. Ritsema, Organization for Scientific Research in Indonesia, No. 46.
27. H. Honda, "Seismic waves", (in Japanese) (1942, Tokyo).
28. F. A. Lindemann, Phys. Zeits., **11** (1910) 609.
29. J. Verhoogen, Trans. Amer. Geophys. Union, **35** (1954) 85.
30. H. Haalck, Zs. f. Geophys., **14** (1938) 111.
31. T. Rikitake, Bull. Earthq. Res. Inst., **27** (1949) 17; **30** (1952) 13.

Abuyama Seismological Observatory,
Faculty of Science,
Kyoto Uuiversity,
Kyoto,
JAPAN.

INDEX OF AUTHORS TO VOLUME XXVII

PAGE

Fujikawa, H. (see **Tomotika, S.** and **Fujikawa, H.**) 145

Fujikawa, H. (see **Tomotika, S.** and **Fujikawa, H.**) 227

Ichinohe, T. Study on Change of Gravity with Time. Part I. On the Tidal Variation of Gravity. 289

Ichinohe, T. -Study on Change of Gravity with Time. Part II. Repeated Gravity Surveys in the Kinki District. 317

Inoue, Y. -The Vertical Distributions of the Temperature and Density in the Lower Ionosphere. 67

Ishida, Y. (see **Takahashi, I., Ishida, Y.** and **Ôta, M.**) 41

Ishida, Y. (see **Takahashi, I.** and **Ishida, Y.**) 47

Ishii, K. (see **Kiho, H.** and **Ishii, K.**) 23

Kiho, H. and **Ishii, K.** -On the Glide Twinning in Single Crystals of Tin. 23

Kishimoto, Y.—Seismometric Investigation of the Earth's Interior. Part I. On the Structure of the Earth's Upper Layer. 125

Kishimoto, Y.—Seismometric Investigation of the Earth's Interior. Part II. On the Structure of the Earth's Crust. 243

Miki, H.—On the Earth's Mantle. 363

Nishioka, S.—On a New Method of Measuring Specific Heat of Metals. 31

Nishioka, S. -Effects of Cold Working on Specific Heat of Metals. 35

Ôta, M. (see **Takahashi, I., Ishida, Y.** and **Ôta, M.**) 41

Takahashi, I., Ishida, Y. and **Ôta, M.** -A New Method of Measuring Ultrasonic Sound Velocities in Liquids. 41

Takahashi, I. and **Ishida, Y.** Determination of Ultrasonic Sound Velocities and Elastic Constants of Solid. 47

Takasu, K. -Microclimatic Study, II. A New Type Thermojunction for Microclimatic Use. 55

Takasu, K. -Microclimatic Study, III. A Working Method for finding Austausch Coefficients from the Records of Temperature Fluctuations. 59

Tashiro, K. -Vectorial Stability Criteria of the Feed-back Physical System. Part. I. . 157

Tashiro, K. -Vectorial Stability Criteria of the Feed-back Physical System. Part. II. . 185

Tomotika, S. -A Note on the Skin Friction of a Flat Plate to Oseen's Approximation. 1

Tomotika, S. and **Yosinobu, H.**—The Drag on an Elliptic Cylinder moving in a Viscous Liquid at Small Reynolds Numbers. 11

Tomotika, S. and **Fujikawa, H.** -An Expansion Formula for the Lift on a Circular-arc Aerofoil in a Stream bounded by a Plane Wall. 145

Tomotika, S. and **Fujikawa, H.**—The Influence of Vortices upon the Drag experienced by an Elliptic Cylinder moving through an Inviscid Liquid. 227

PAGE

Uchida, Y. and **Yagi, H.** Spectra of Coloured Lithium Fluoride Crystals. 357

Yagi, H. Some Remarks on the Operation of the Self-controlling Infra-red Spectrophotometer. 335

Yagi, H.—Changes of Absorption Bands of Alkali-halide Crystals coloured in Several Conditions. 347

Yagi, H. (see **Uchida, Y.** and **Yagi, H.**) 357

Yoda, W.—On the Magnetic Anomalies and their Secular Variations around Maeyama on Simabara Peninsula. 101

CONTENTS

Changes of Absorption Bands of Alkali-halide Crystals coloured in Several Conditions

By Hisao Yagi 347

Spectra of Coloured Lithium Fluoride Crystals

By Yôichi Uchida and Hisao Yagi 357

On the Earth's Mantle

By Haruo Miki 363

Printed by NIPPON INSATSU SHUPPAN

Fukushima, Osaka